Tomographic Study of Pulsar Magnetosphere using RRI-GBT Multi-Band Receiver

Thesis

Submitted in partial fulfilment of the requirements of
BITS F421T

By

Shetgaonkar Hrishikesh Digambar
(2014B5A70681P)
Department of Physics
BITS Pilani, Pilani Campus

Under the supervision of
Avinash Deshpande
Professor
Astronomy and Astrophysics Department
Raman Research Institute

Co-supervisor:
Dr. Kaushar Vaidya
Assistant Professor
Department of Physics
BITS Pilani, Pilani Campus

BIRLA INSTITUE OF TECHNOLOGY AND SCIENCE, PILANI (RAJASTHAN)

December 1, 2018

ACKNOWLEDGEMENT

I am immensely grateful to my supervisor Prof. Avinash Deshpande for not only giving me this opportunity to work under his expert guidance, but also for his constant support and patience throughout last four months. His availability at any time of the day (even night!), encouragement towards overcoming challenges and focussing immensely on my learning rather than completing a set of tasks is what I respect and am thankful for. Moreover, he shared with us his experiences which has inspired me and helped me grow over the past four months.

I am wholeheartedly thankful towards Dr. Kaushar Vaidya who is my co-supervisor for her encouragement and support. I would also like to thank the Department of Physics, BITS Pilani, Pilani Campus for giving me an opportunity to pursue my interest in pulsars.

I also thank Raman Research Institute for not only giving me the opportunity under 'Visiting Student Program' but also for providing necessary resources. The flexibility of timings at the institute allowed me to work more efficiently.

I would also like to thank my family. Nothing would have been possible if not for their unconditional support and patience. Last but not least, I also thank new friends that I made here, especially my lab mates Akhil and Aleena.

CERTIFICATE

This is to certify that the Thesis entitled "Tomographic Study of Pulsar Magnetosphere using RRI-GBT Multi-Band Receiver" and submitted by Mr. Shetgaonkar Hrishikesh Digambar ID No. 2014B5A70681P in partial fulfilment of the requirement of BITS F421T Thesis embodies the work done by him under my supervision.

Signature of the Supervisor

Avinash Deshpande
Professor
Astronomy and Astrophysics Department
Raman Research Institute

ABSTRACT

The sub pulse modulation in pulsars can be used to construct a polar emission map at a particular frequency. The well accepted Radius to Frequency mapping which gives a relation between the frequency of emission and the height in the magnetosphere for pulsars can then be used to determine the height of these emission maps. The RRI-GBT Multi-Band Receiver, capable of simultaneous observations in 10 discrete frequency bands ranging from 100 to 1500 MHz can be used for this purpose. This tomographic study of pulsar magnetosphere can help us get a better understanding of the emission mechanisms in pulsars.

List of Abbreviations

- RRI: Raman Research Institute
- GBT: Green Bank Telescope
- MBR: Multi Band Receiver
- RF: Radio frequency
- IF: Intermediate Frequency
- LO: Local Oscillator
- GPS: Global Positioning System
- Stokes I, Q, U, V: Stokes Parameter (detailed description in text)
- DM: Dispersion Measure
- SNR: Signal to Noise Ratio
- P or P_1: Rotation period of pulsar
- cP_1^{-1}: cycles per rotation period
- HRF: Harmonic Resolved Fluctuation
- LRF: Longitude Resolved Fluctuation

Contents

1.1 What are Pulsars?

Ever since their discovery in 1967 by Jocelyn Bell; a graduate student working at the Mullard Radio Astronomy Observatory in Cambridge, pulsars have continuously been interesting as well as enigmatic. The highly periodic pulse signals were so puzzling at the time that there were even serious suggestions to associate them with intelligent alien civilizations. But over the years, many such objects having short periodic bursts, mostly in in radio part of the electromagnetic spectrum were discovered which helped us develop a better understanding and conclude that the signals are of astrophysical origin instead of alien civilizations.

Today, pulsars are understood to be special type of neutron stars. They are rapidly rotating and highly magnetized with a misalignment in its magnetic and rotation axis. Their radius is of the order 10 kilometres. These are formed when stars run out of nuclear fuel and their core collapses under gravity. During the core-collapse, conservation of angular momentum increases the rotation rate while conservation of magnetic flux gives rise to strong magnetic fields ($\approx 10^{15}$ Gauss). Acceleration of charged particles to ultra-relativistic velocities in these strong magnetic fields form emission beams (mostly in radio region) which are aligned along the magnetic axis. These beams, when not aligned with the rotation axis leads to "light-house" effect as it sweeps past our line of sight once per rotation. Fig (1.1) is a schematic diagram explaining this phenomenon.

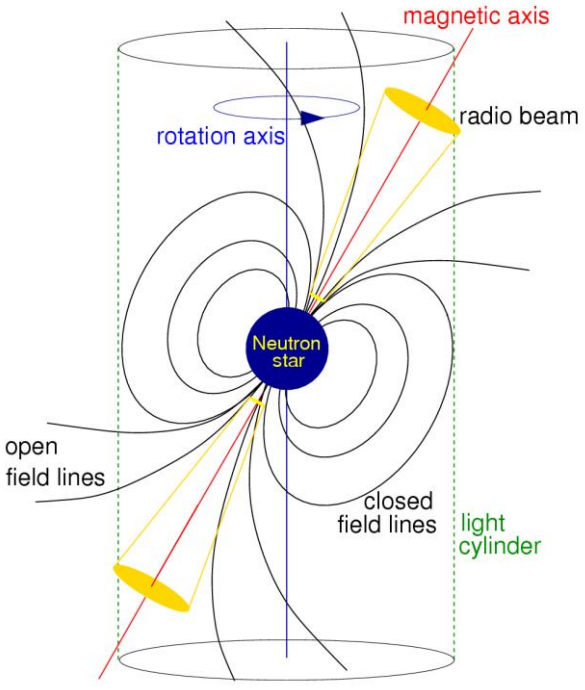

Fig 1.1: Pulsar
source: https://www.cv.nrao.edu/course/astr534/Pulsars.html

After over 50 year of pulsar research, we have come a long way in understanding these special but enigmatic objects. But still, we don't know enough and pulsar research is in its infancy. There are many mysteries and unanswered questions revolving around pulsars. Apart from the general human zeal to explore the unknown, pulsars provide a very good laboratory to study extreme conditions which are very difficult to be achieved locally on Earth. Decoding the information present in pulsed signals is an exciting challenge which when solved, can help us develop a better understanding for neutron stars.

Pulsars have extremely stable periods. The milli second pulsars are believed to be more accurate than the best clocks we have managed to develop. Hence pulsars can now be used as time keeping instruments to study other phenomena. Pulsar Timing array is one such initiative to probe gravitational waves using pulsars. Moreover, the work by Hulse and Taylor on a pulsar-neutron star binary B1913+16 for which they received a Noble Prize in 1993, is a prime example of how pulsars were used to indirectly verify Einstein's General Relativity and existence of gravitational waves.

1.2 Some pulsar properties

- Period:
  - Period of a pulsar is defined as the time interval between two consecutive pulses. Generally, the period can vary from milliseconds to seconds. It is observed that pulsars slow down gradually over time.

- Average/Integrated profile:
  - Pulsar signals are generally very weak. Most of the time, the pulse signals are buried in noise and the peaks are not always clearly visible in time sequence. However, if many pulsar periods are averaged, the random noise decreases and the peak becomes visible. Even though individual pulses vary, the average pulse profile for a pulsar is quite stable and unique.

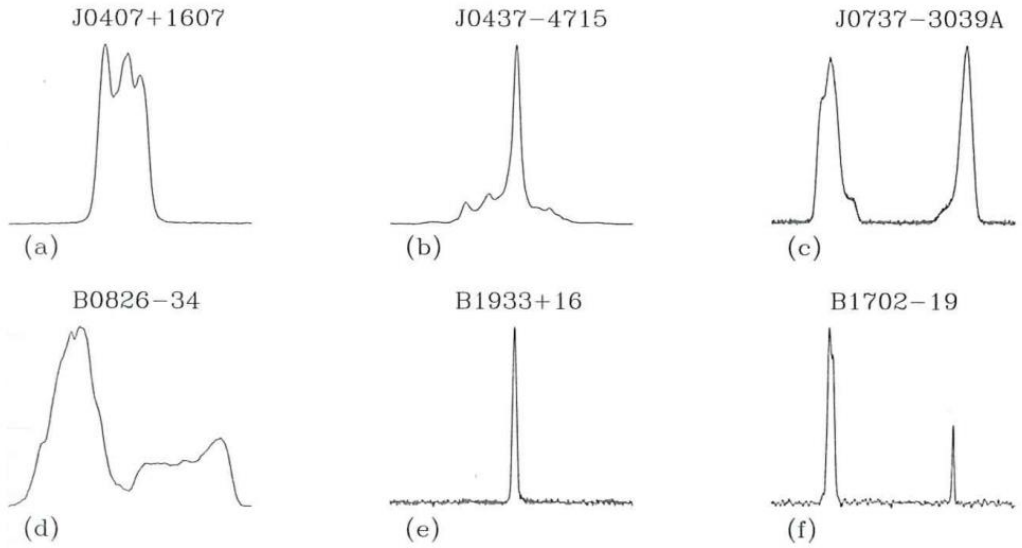

Fig 1.2: Average Pulse profiles for some pulsars
Source: "Handbook of Pulsar Astronomy", Lorimer & Kramer

2. Emission Mechanisms and Drifting sub pulses:

2.1 Acceleration of charged particles:

The radio pulses have origin in the dipolar magnetosphere of pulsar. The non-thermal spectrum and high value of brightness temperature suggests need for coherent emission mechanism. Goldreich and Julian (1969) proposed a simple pulsar model where the magnetic and rotation axis of the neutron star were aligned. With angular velocity $\boldsymbol{\Omega}$ and dipolar magnetic field $\boldsymbol{B}$, there would be a co-rotating magnetosphere within the light cylinder filled with a charge density:

$$\rho_e = \frac{-\boldsymbol{\Omega}.\boldsymbol{B}}{\boldsymbol{2\pi c}} \times \frac{1}{1-\frac{\Omega^2 r_\perp^2}{c^2}}$$

Where $r_\perp = r\sin(\theta)$ and θ is polar angle.

This distribution of charges in the co-rotating magnetosphere is such that the $\boldsymbol{E.B} \sim 0$. This means the electric field along magnetic field lines is zero and acceleration of charge particles does not occur.

Fig (2.1) shows a sketch of Goldreich and Julian (1969) model. Note the alignment of rotation axis($\boldsymbol{\Omega}$), magnetic axis($\boldsymbol{B}$), charge distribution (**+/-**) and currents($\boldsymbol{J}$). The dashed line is where $\cos(\theta) = \pm\frac{1}{\sqrt{3}}$ i.e., Ω.B = *0*. This line separates regions of positive and negative charge.

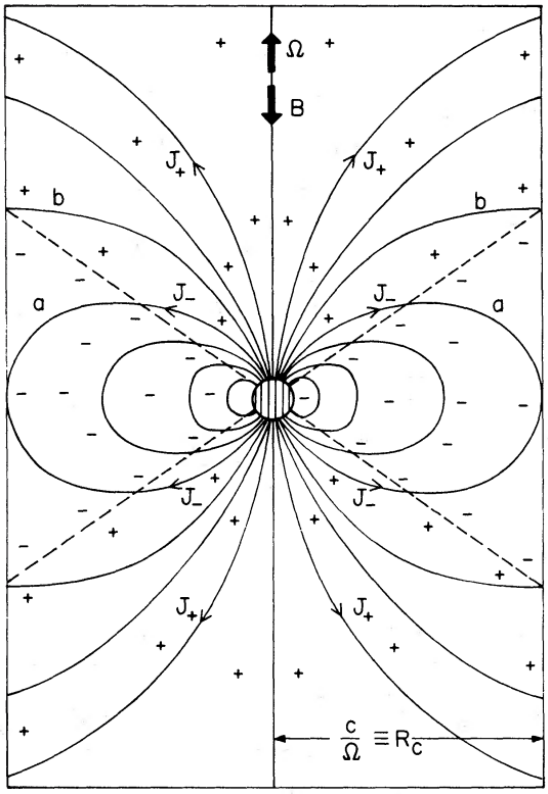

Fig 2.1 Goldreich and Julian (1969) model for pulsar magnetosphere
Source: "Theory of Pulsars", Ruderman and Sutherland (1975)

However, near the poles polar gaps are formed. These polar gaps are regions in magnetosphere with zero charge. Here ***E.B*** is not zero and hence acceleration of charges to ultra-relativistic velocities can occur. This produces electromagnetic radiations. The gap height is limited by vacuum breakdown. Any gamma-ray photon (which was produced by primary charged particle accelerated in the magnetic field) with sufficient energy may interact with the strong magnetic field in the gap to produce more electron-positron pairs. These pairs are again accelerated to ultra-relativistic energies where they produce electro-magnetic radiation. Hence, these sparks feed relativistic charges into localized bundles (columns) of open magnetic field lines.

2.2 Drifting sub-pluses

Although the average pulse profile is a very unique signature of any pulsar, individual pulses are different and can be made of multiple components. The sub pulse structures were initially studied by Backer (1973) and can tell us a lot about the emission regions in the pulsar magnetosphere which can be associated with columns of localized bundles of relativistic charges in the magnetosphere. Fig 2.2 describes the drifting sub pulse phenomenon. The vertical axis is the pulse number while the horizontal axis is longitude (where a longitude of 360deg corresponds to one complete period). It also shows the integrated profile at the top which lacks any information of the drifting sub-pulses.

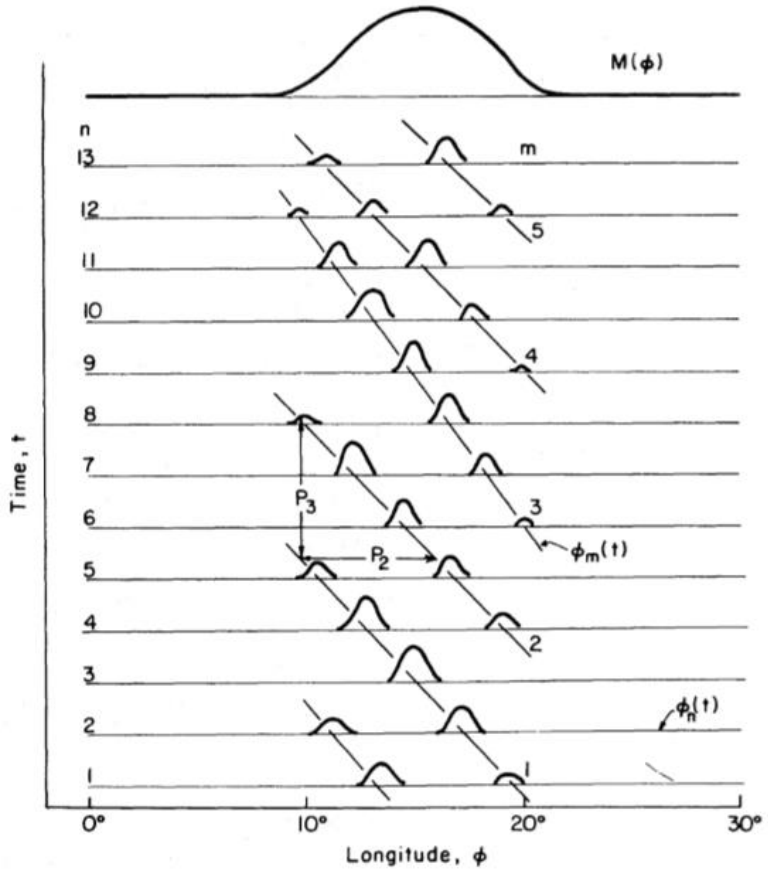

Fig 2.2: Drifting Sub Pulse
Source: Becker (1973)

These sub pulse components can be mapped to individual emission components in the pulsar magnetosphere as shown in Fig 2.2.

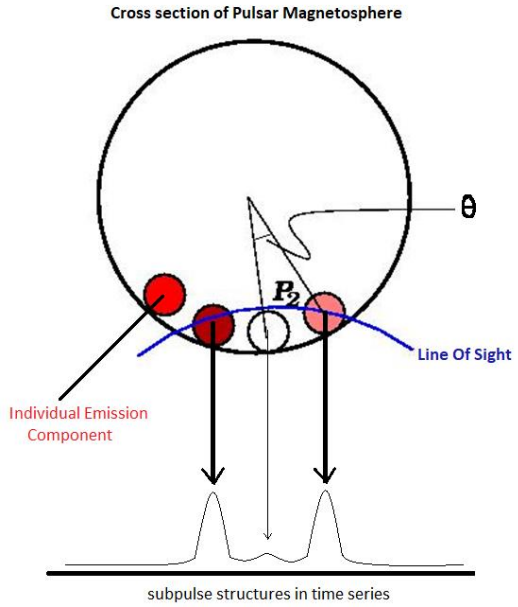

Fig 2.2 Mapping of emission components to sub pulse in time sequence

Hence, studying such sub-pulses can be used to construct a polar emission map at the frequency of observation. Moreover, in pulsars it is observed that the frequency of radio emission varies with the height in magnetosphere. Higher frequencies are emitted closer to the surface of the neutron star. This relation is the well accepted 'radius-to-frequency mapping' and can be used to determine the height of this emission map.

Simultaneous observations in multiple frequency bands can be used to build such emission maps at different heights. Temporal variation of these polar emission maps and correlating two emission maps can help us get a better understanding for emission mechanisms in pulsars.

3. Data Analysis

3.1 Data:

The multi frequency data were recorded using RRI-GBT Multi-Band Receiver (MBR). The MBR is capable of simultaneous observations in 10 discrete frequency bands ranging from 100 to 1500 MHz and the MBR data are recorded in '.mbr' files. Table 3.1 shows the bright drifter pulsars selected for the study.

Sr No.	Name	RAJ	DECJ	Dist(kpc)	Flux(mJy)@ 400MHz
1	B0031-07	34:08.9	-07:21:53.409	1.03	52
2	B0329+54	32:59.4	+54:34:43.57	1	1500
3	B0809+74	14:59.5	+74:29:05.70	0.43	80
4	B0818-13	20:26.4	-13:50:55.859	1.9	102
6	B0834+06	37:05.6	+06:10:14.56	0.19	89
7	B1929+10	32:13.9	+10:59:32.420	0.31	303

Table 3.1: Bright Drifter Pulsars

For initial data analysis, we shall focus on a bright drifter "B0809+74". The data were recorded on 25th July 2009.

- Data Format:
  Each mbr data file is made up of 2,027,520 mbr packets. The mbr packet is 1056 bytes long. The first 32 bytes in mbr packet is the header and stores information like Observation ID, Source Name, Local Oscillator (LO) frequency, GPS count, packet count, etc. and the structure of its header is shown in Fig 3.1. The 1024 bytes after the header contain raw voltage data sampled at 33 MHz. Of these 1024, 512 bytes are for X polarization and Y polarization each.

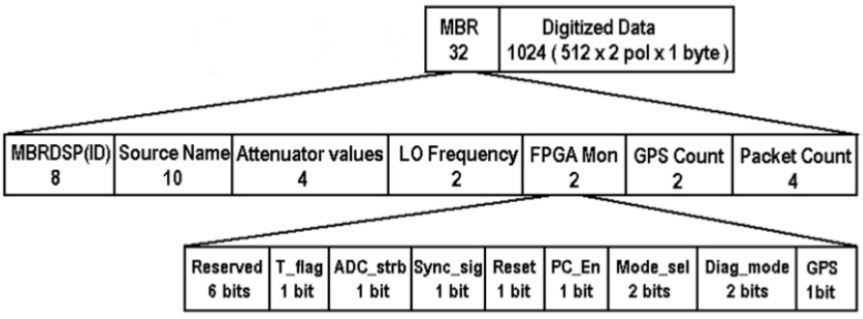

Fig 3.1: MBR packet header

Each observation band is 16 MHz wide and the central frequency of this band can be calculated from LO frequency by using the formula RF = LO ± IF. Of these two values select the one which lies in the band. The LO, IF and resulting RF (central frequency) values obtained for 8 channels is given in Table 3.2

Channel Number	IF (MHz)	LO (MHz)	Central Frequency (MHz)
1.	70	190	120
2.	70	242	172
3.	140	373	233
4.	140	470	330
6.	140	758	618
7.	140	870	730
8.	140	950	810
9.	140	1030	1170

Table 3.2: Central Frequency for channels

The recorded data also suffer from missing packets. These missing packets can be considered as bad data and are flagged (given a value -9999 in dynamic spectrum) so that they can be avoided while calculating time sequence. The missing packets were detected by keeping a count of number of packets read and comparing that to the packet number present in the header of current packet being read. The missing data can be seen as dark blue solid patches in dynamic spectra (Fig 3.4).

3.2 Synchronization

For analysing signals received across all 10 frequency bands, it is extremely important that we synchronize the data from each band. This would ensure that we compare and study pulse signals from different channels having the same origin at the pulsar. Apart from taking care of propagation delays like dispersion delay, it is also important that we do synchronization at the packet level.

For this, the header of each packet is analysed and the GPS count, packet number and GPS pulse for each packet is recorded. GPS count is the number of seconds after 00:00hrs on the day of observation. The count is updated every second. GPS pulse is a very short (nano seconds) pulse. If this pulse is 'high' while writing the header, 1 is recorded in the GPS bit. Else zero is recorded. Plot the GPS count vs Packet Number for all packets and fit a line through those with 'high' GPS bit. Let us call this line 'A'. Refer Fig 3.2

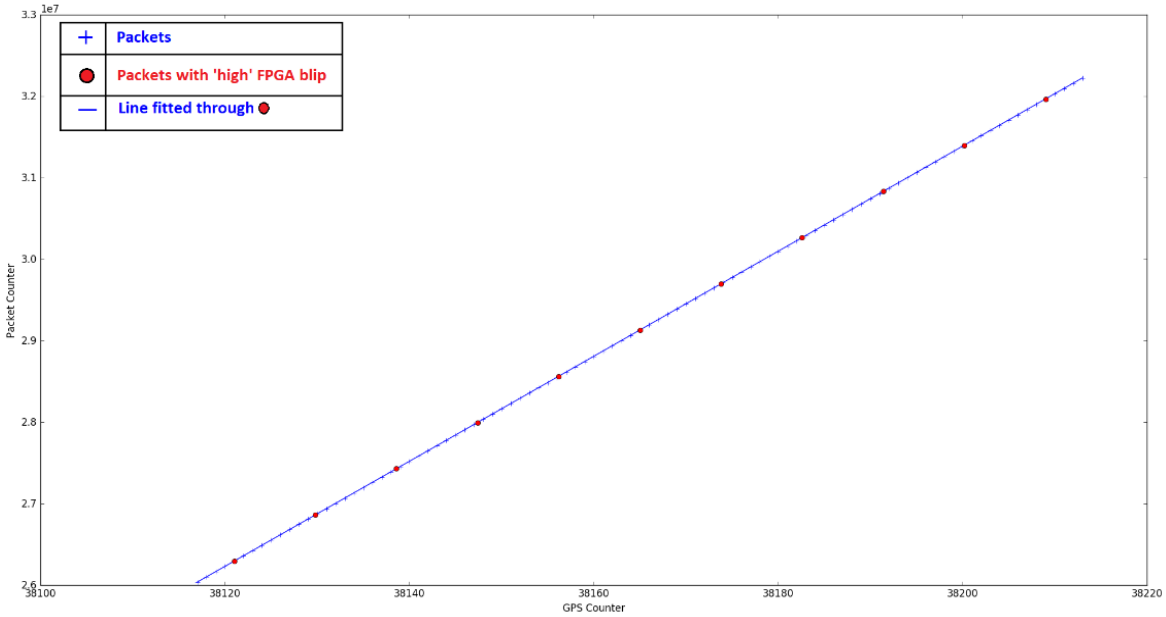

Fig 3.2: GPS counts vs Packet Number
The packet with 'high' GPS pulse in header is marked in red

Such analysis is done for all 9 channels. Now taking the first occurrence of GPS count as a reference start for our observation, note the corresponding packet number on the line 'A' for all channels. Treat this packet number as the first packet for our observations in all corresponding channels.

3.3 Dynamic Spectrum

Dynamic spectrum is simply intensity as a function of frequency and time. It can be constructed by calculating the spectrum (intensity as a function of frequency) at different times. To calculate the spectrum, we take Fast Fourier Transform (FFT) of 512 samples each in X polarization and Y polarization. Let X and Y be the resulting spectrum for x and y polarization. Intensity spectrum for x polarization can be calculated as $(X.X^*)$, where X^* denotes complex conjugate of X. Similarly, intensity spectrum for y polarization can be calculated as $(Y.Y^*)$. Note that the intensity spectrum has 256 channels. The resulting intensity spectrum (Fig 3.3) forms a column of the dynamic spectrum with each column (i.e., spectrum) taken at successive time intervals. Also note that the entire bandwidth of 16MHz is divided into 256 channels. So, each channel is 6.25 KHz wide.

We also calculate cross spectrum as $(X.Y^*)$. Now four Stokes parameters can be calculated as:

$$\boldsymbol{I} = (X.X^*) + (Y.Y^*)$$

$$\boldsymbol{Q} = (X.X^*) - (Y.Y^*)$$

$$\boldsymbol{U} = 2Re(X.Y^*)$$

$$\boldsymbol{V} = -2Im(X.Y^*)$$

Polarization information can be deduced using these four parameters.

Pulsar signals are generally weak; hence we take average of $N_{\_integration}$ such spectral columns for obtaining a better Signal to Noise Ratio (SNR).

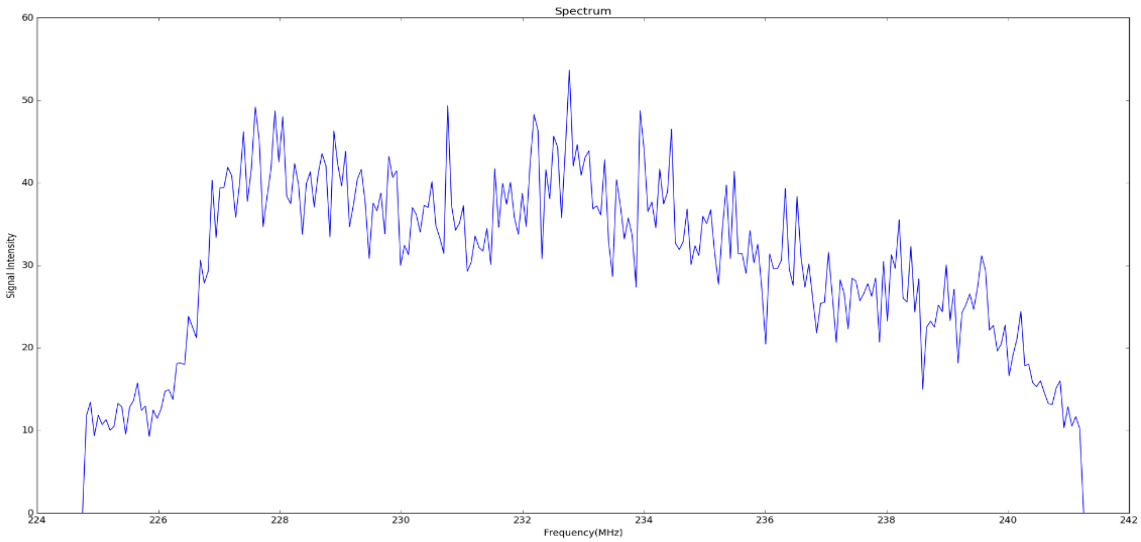

Fig 3.3: Spectrum

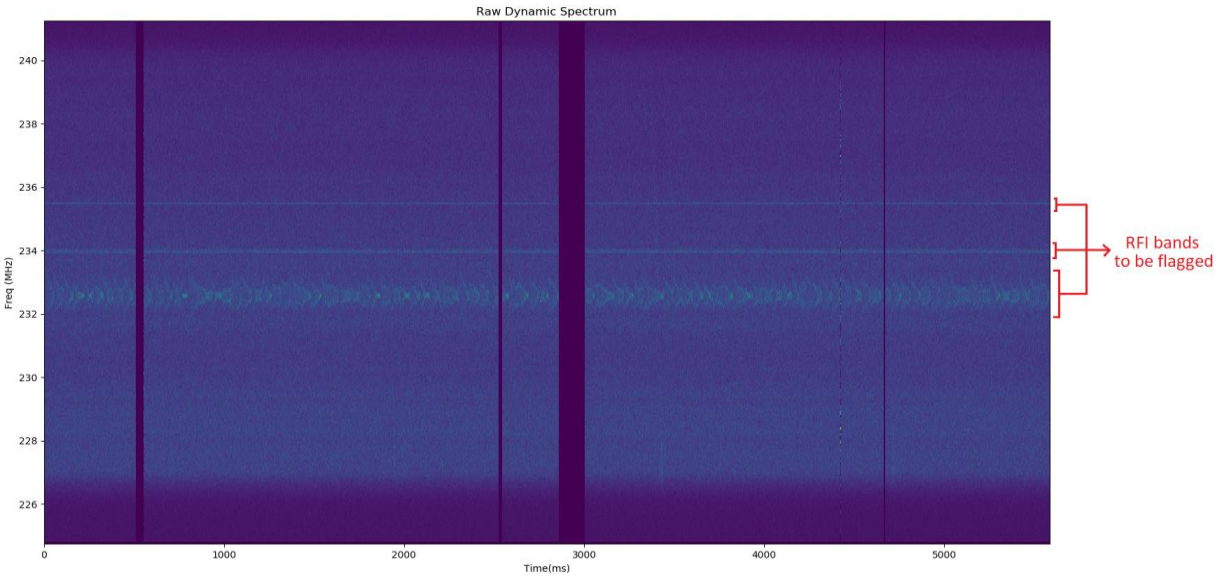

Fig 3.4: Dynamic Spectrum for 6 sec data

This packet synchronized and integrated dynamic spectrum is generated for the entire observation and is saved as a '.spec' file for further processing.

3.4 Removing Bad Channels:

Looking at the Dynamic Spectrum, we can see strong and continuous signals in some channels. These signals are Radio Frequency Interference (RFIs). They are of terrestrial origin and corrupt our data. Hence is necessary that we detect and remove such signals before moving on to pulsar analysis.

Random noise in signal is Gaussian in nature. Hence, the power spectrum, which is the square of the signal would be exponential in nature. For an exponential distribution, the mean is same as the root mean squared error. We can use this property to detect any non-Gaussian nature in our dynamic spectrum.

Thus, we can now use the non-Gaussian nature of RFIs is used to detect them. First a workable chunk of Dynamic Spectrum is selected from the large '.spec' file. For this, mean and root mean squared error is calculated for good (un-flagged) data for all 256 channels. Further, efficiency for channel ch_i is calculated as:

$$efficiency[ch\_i] = \frac{mean[ch\_i]}{rms[ch\_i]} \times \frac{1}{\sqrt{N\_integration}}$$

This efficiency is calculated for all 256 channels. Fig 3.5 shows a sample efficiency plot. If the signal in a channel follows Gaussian nature, its efficiency is expected to be unity. Any deviation from unity hints to non-Gaussian behaviour of signal. At this point, it should be noted that the signals in each channel does not approach unity because the presence of pulsar signal in the data itself introduces non-Gaussian behaviour. RFIs however introduce significant amount of deviation from unity and can be thus detected and data in corresponding channels be flagged to -9999.

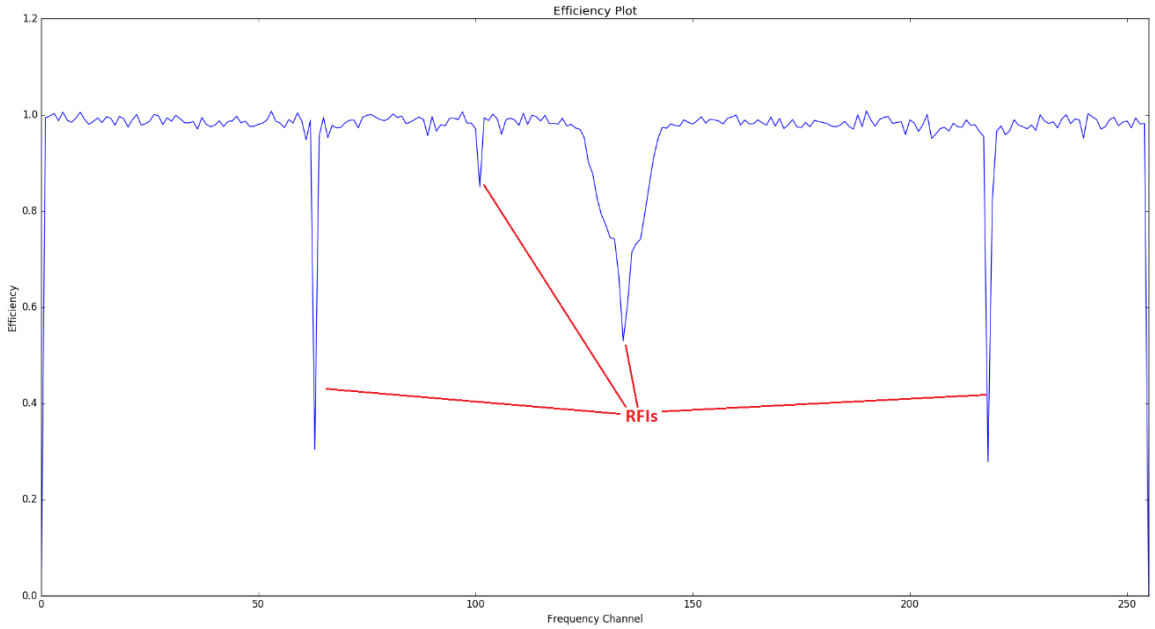

Fig 3.5: Efficiency Plot. Note the RFIs with large deviation from unity

We also reject first and last 10 channels (i.e. ch 01 to 10 and ch 246 to 255) due to their low gain. The data in these channels is flagged to -9999.

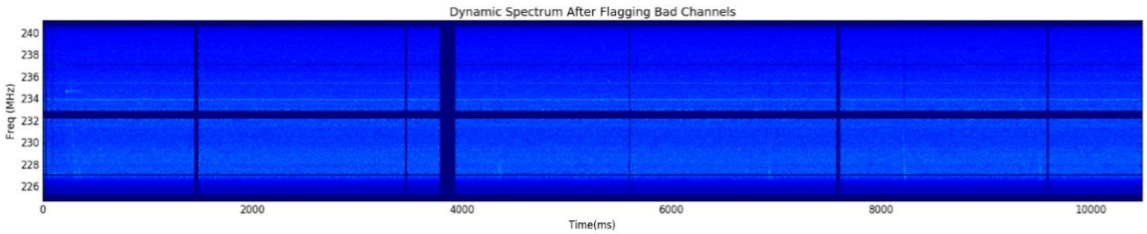

Fig 3.6: Dynamic Spectrum with flagged rejected channels (dark blue solid patches)

3.5 Subtracting Robust Mean:

Robust mean for a particular channel can be defined as the mean intensity of all data in that channel excluding the data which are part of the pulsar pulse signal. The robust mean is calculated for all 256 channels and is then subtracted from the corresponding channel in the dynamic spectrum.

3.6 De Dispersion

As the pulsar signal propagates through Interstellar Medium to reach us, it interacts with intervening charged particles and suffers from dispersion. Dispersion occurs because the refractive index of intervening medium is frequency dependent. Lower frequency radiations travel slower than higher frequency radiation. Hence pulses at lower frequency are delayed. As a result, even if the pulsar produces signals at all frequencies at the same time, we would receive higher frequency pulse earlier than the lower frequency pulse.

The dispersion delay is between signals at two frequencies is given by the formula:

$$\tau_{delay} = \left(4.15 \times 10^6 \times \left(\frac{1}{\nu_{low}^2} - \frac{1}{\nu_{high}^2}\right) \times DM\right) \; milliseconds$$

Here ν_{high} and ν_{low} are higher and lower frequencies in MHz. *DM* is a constant called Dispersion Measure. Its units are pc cm^{-3}. By knowing the electron density $(n_e \, \mathrm{cm}^{-3})$ distribution between us and the pulsar and distance to the pulsar in parsecs(D), DM can be calculated using the relation:

$$DM = \int_0^D n_e \, dl$$

Since we know the time delay between pulses occurring at two frequencies, the dispersion effect can be nullified by just shifting the lower frequency signals earlier in time by an amount τ_{delay} milliseconds. This is required to be done for all 256 channels in the 16 MHz bandwidth and this process is called De-Dispersion.

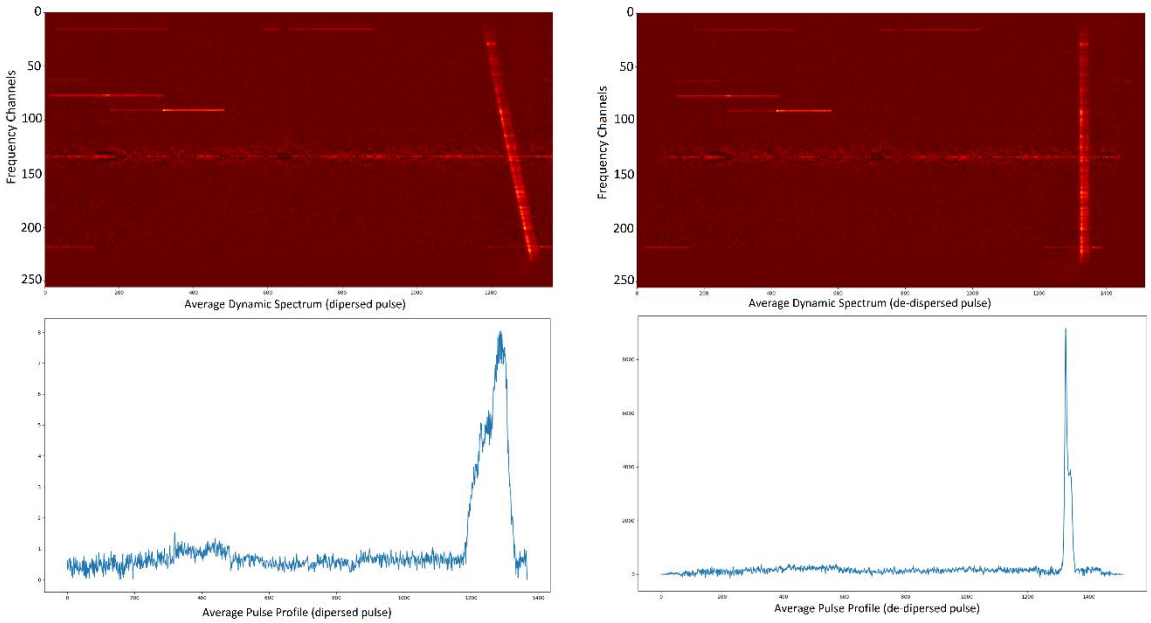

Fig 3.7: Dispersed pulse and its frequency integrated average pulse profile is seen on the left while the de-dispersed pulse and its average pulse profile is seen in the right.
Note the increased Signal to Noise Ratio (SNR) for de-dispersed pulse.

3.7 Time Sequence:

After flagging all bad data and correcting for the dispersion delay in Dynamic Spectrum, we can now integrate along all frequency channels to get average intensity as a function of time. Such a plot is called time sequence. While taking average, it is important to reject the bad data flagged earlier. Fig 3.8 is a time sequence plot for n seconds for pulsar B0809+74 in frequency band 224.75 MHz to 241.25 MHz.

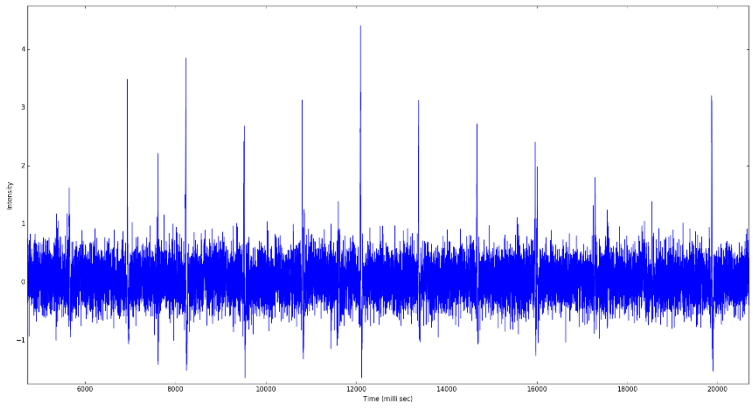

Fig 3.8: Time Sequence for B0809+74 after baseline subtraction with pulse peaks. Notice the negative intensities. Most are due to random variations(noise) about the baseline. The more intense dips near pulses are due to compression.

To see the drifting sub pulses, a single pulse stack was plotted. A pulse stack simply dividing the entire time series data into small chunks where each chunk is exactly one time period long. Stack these successive chunks in rows to obtain a graph where the vertical axis is period number while horizontal axis is longitude (360 deg in longitude corresponds to one complete period).

Fig 4.1 shows the single pulse stack for Pulsar B0809+74 band 3 over 55 periods. We can clearly see the drifting sub pulse.

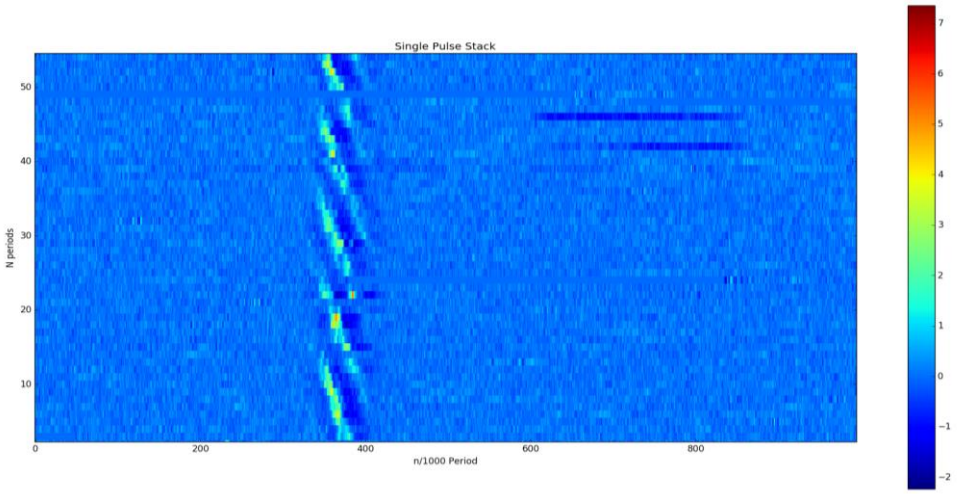

Fig 4.1: Drifting sub-pulse in Single Pulse Stack for 55 periods in pulsar B0809+74

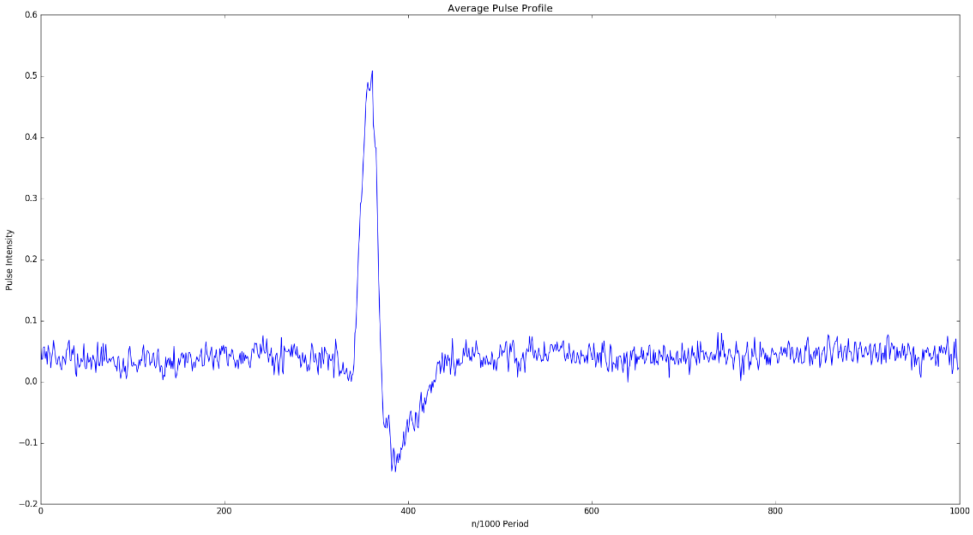

Fig 4.2: Note the dip after the pulse due to compression

The pulse stack can be integrated over vertical axis to obtain an average pulse profile. In doing so, we realise that the intensity near the pulse becomes negative (Fig 4.2). This happens because of compression of signal. In the presence of a strong signal (pulse), the amplifier gain function deviates from its linear nature to enter non-linear regime. Due to this, compression in the intensity across the spectrum takes place.

Compression only occurs in the on-pulse region due to the strong pulse signal. The fact that the off-pulse region does not suffer from compression can be used to correct it in the on-pulse region. This process is called De-compression and is done by comparing the selected sections of on-pulse spectrum with corresponding part of off-pulse spectrum. Treating the latter as reference, we determine the factor by which the on-pulse spectrum needs to be corrected. In the on-pulse spectra, only that part is selected which does not contain pulsar signal.

5. De – Compression

5.1 What is Compression?

As discussed in the previous section, compression occurs due to the presence of a strong signal in the observed frequency band. In ideal conditions, the amplifier gain function is expected to be linear. This means the output varies linearly with the input. However, for a strong signal, which happens to be the pulsar signal in our case; the amplifier gain function enters a nonlinear regime and the output is less than what is expected. As a result, the signal strength observed across the entire spectrum is less than what it truly is. In the average dynamic spectrum of band 3 for pulsar B0809+74 taken over nearly 600 seconds of data (refer Fig 5.2). This drop in the intensity is clearly seen as a dark red patch in the off-pulse region of spectrum containing the strong signal (pulse). It is necessary that this drop in the signal strength be corrected for before proceeding to further analysis.

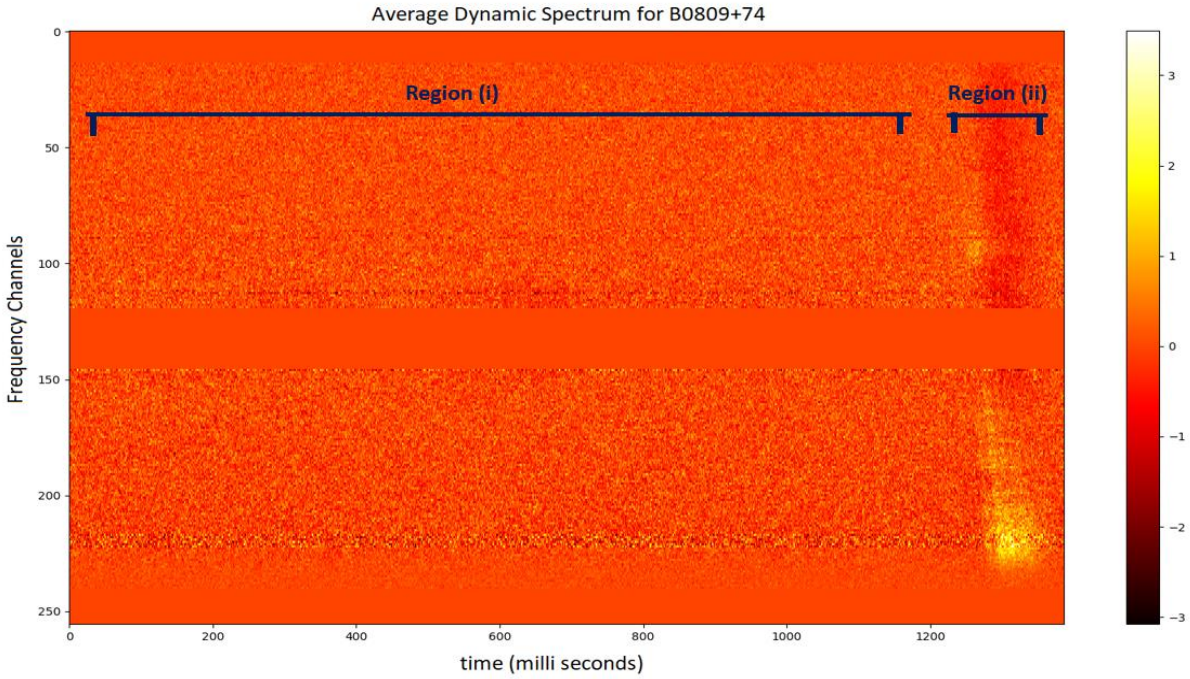

Fig 5.2: Average Dynamic Spectrum for B0809+74 for 600 sec data.
De-compression is seen as a dark red patch near the pulse.

5.2 How to De-compress?

De-compression can be achieved by simply comparing the signal strength in the off-pulse region of spectrum containing the pulse (spectrum in region ii) with that of a spectrum not containing the pulse (average of spectra in region i). From this comparison, we obtain an appropriate factor which we then multiply with the affected region to scale up its intensity. This way, the compressed intensity is boosted to be comparable to that in region ii.

I shall now discuss four methods used for de-compression. In my discussion, I shall talk about how these methods were implemented, why they were expected to work and more importantly; when and where they failed.

(Note that all the rejected data, i.e. data flagged to -9999 in prior processing is not included in calculating robust mean, sum or any other calculations in all the methods discussed below.)

5.3 De-compression Method 1 – Spectral Gain Flattening of Dynamic Spectrum:

For a significantly large chunk of dynamic spectrum (approximately 10 seconds in my case), produce a template spectrum by computing the robust mean across all channels. Robust mean ensures that signal from the pulses (and other strong signals) are excluded while taking the mean. In other words, the intensity in each channel of the template spectrum produced is the mean of all off-pulse intensities in that particular frequency channel of the dynamic spectrum chunk. Hence, we have a template spectrum with intensity as a function of frequency channels. Let this be represented by $T(f)$. The chunk of dynamic spectrum is simply intensity as a function of frequency channels (rows) and time(columns). Let it be represented as $I(f,t)$. Fig 5.3 shows such a dynamic spectrum and its corresponding template spectrum. Mathematically,

$$T(f_i) = \langle I(f_i, t_j) \rangle_{t_j}$$

Here, $\langle A(x,y) \rangle_x$ represents the robust mean of A along x.

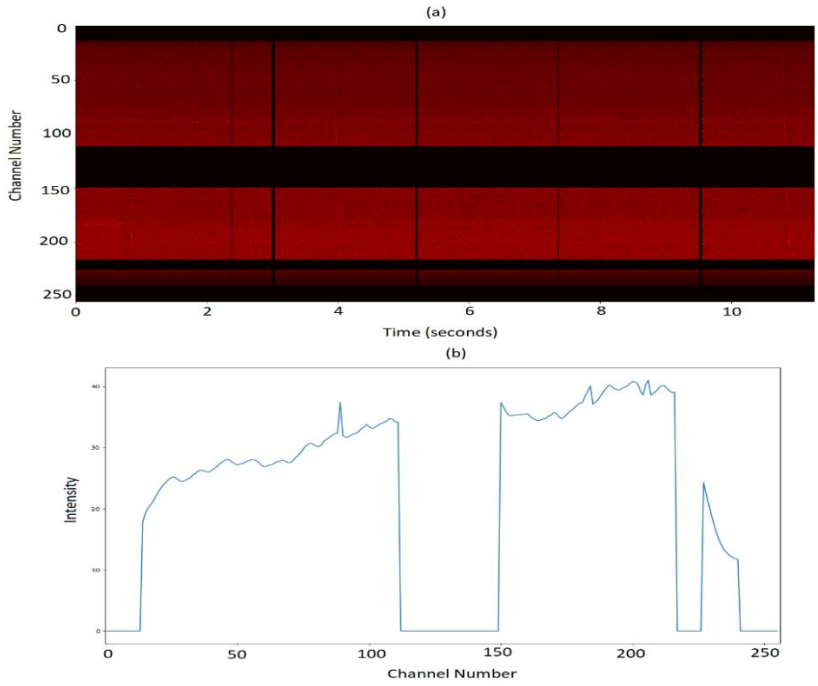

Fig 5.3: (a)Sample Dynamic Spectrum and corresponding (b)Template Spectrum

We now create a spectral gain flattened dynamic spectrum $S(f,t)$ for this chunk where the dynamic spectrum intensity in each frequency channel at all particular time is divided by the template spectrum intensity in the same frequency channel. This is done for all time. Mathematically, this can be represented as:

$$S(f_i, t_j) = \frac{I(f_i, t_j)}{T(f_i)}$$

Here, f_i and t_j represent the i^{th} frequency channel and j^{th} time column respectively.

Hence, the intensities are now normalized to unity with slight deviations in off-pulse (or more precisely off-"strong signal" regions). The pulsar signals have normalized intensity greater than unity while the region suffering from compression has normalized intensity less than unity.

Now, we calculate the robust mean of intensities of the spectral gain flattened dynamic spectrum across each time column. The robust mean ensures that only the off-pulse part of the spectrum is included while calculating mean. This gives a correction factor at each time. Thus, we have correction factor $c(t_j)$ as;

$$c(t_j) = \langle S(f_i, t_j) \rangle_{f_i}$$

This correction factor is near unity for all t_j in the off-pulse region while for t_j with the pulse, it is less than unity. Dividing the original dynamic spectrum by this correction factor give the de-compressed dynamic spectrum:

$$I_{\text{de-compressed}}(f_i, t_j) = \frac{I(f_i, t_j)}{c(t_j)}$$

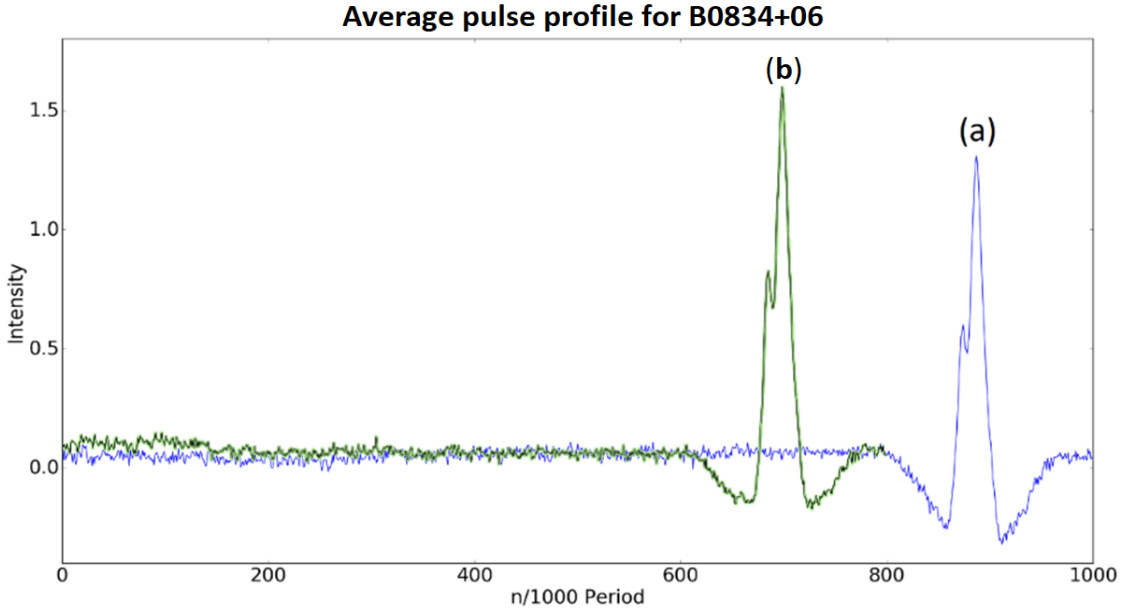

Fig 5.4: (a) Average Pulse Profile for B0834+06 (a) before de-compression shown in blue. (b) after de-compression by method 1 shown in green with same baseline (shifted to the left avoid overlap). Note that this de-compression is not sufficient which led us to develop method 2.

The integrated pulse profile before and after de-compression are shown in Fig 5.4(a) and Fig 5.4(b) respectively. As clearly visible this method was not successful in de-compression and managed to fix the decrease in intensity very slightly. This can be due to two reasons:

1. The robust mean might not be that robust in excluding all signals belonging to the pulsar.
2. Due to a low Dispersion Measure which would manifest as a low dispersion delay, at any particular time, the spectrum is more likely to be dominated by on-pulse signals and the robust mean calculated would actually be that of on-pulse region rather than the off-pulse region.

5.4 De-compression Method 2 – Detecting spectrum peak and rejecting nearby channels:

In this method, we produce template spectrum $T(f)$ as discussed in the previous method. Then, for each spectrum $S(f_i)$ (taken at time column t_j) in the dynamic spectrum, we find the frequency channel with peak intensity. Depending on dispersion delay and pulse width, we then flag some (say 25%) of total channels on each side of the peak. For the unflagged channels, we sum the intensities in this spectrum $S(f_i)$ and represent it by $A(t_j)$. Similarly, we also sum the intensities in template spectrum $T(f)$ for the same unflagged channels and represent it by $B(t_j)$. The correction-factor $c(t_j)$ is now simply:

$$c(t_j) = \frac{A(t_j)}{B(t_j)}$$

This correction factor is a measure of how much compression the intensities have suffered and the de-compressed intensities can be obtained by dividing the original dynamic spectrum by these correction factors as done in previous method.

$$I_{\text{de-compressed}}(f_i, t_j) = \frac{I(f_i, t_j)}{c(t_j)}$$

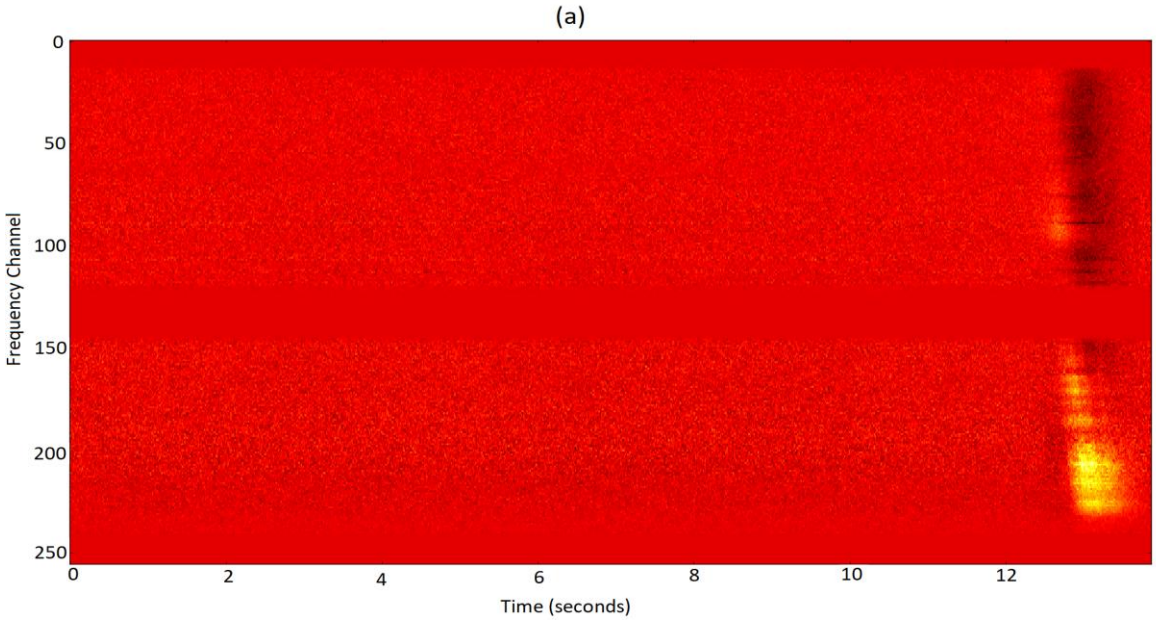

Fig 5.5: Folded Dynamic Spectrum for B0834+06 (a) Before de-compression

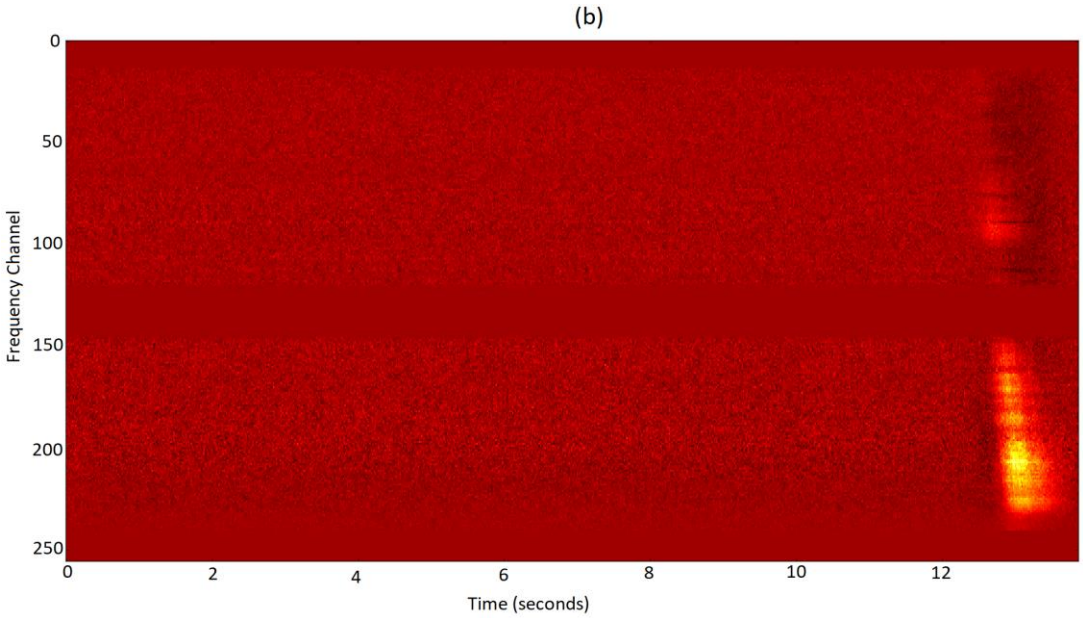

Fig 5.5: Folded Dynamic Spectrum for B0834+06
(b) After de-compression after de-compression by method 2 shown in green.
The dark red/black band is the drop in intensities due to compression. Note that this de-compression too is not sufficient and hence not acceptable.

The average dynamic spectrum (folded over some 500 pulses) for B0809+74 before and after de-compression are shown in Fig 5.5(a) and 5.5(b) respectively. As can be seen, this method is effective at latter part of the pulse when the pulse signal is strong and peak detection is more accurate. It fails at in the region where the pulse is weak. This is likely due to the peak lying elsewhere in the un-folded spectrum.

5.5 De-compression Method 3 – Pulse Position:

The uncertainties in determining which signals belong to the pulsar and which don't is one major drawback of method 1 and method 2. In method 1, there is a high chance that we include the undesired pulsar signal while calculating the correction factor. In method 2, the peak might be due to RFI instead of the pulsar signal. Hence a method which can predict the pulse position in the dynamic spectrum and use this information while calculating the correction factor is desired.

For this, we create a 'pulse mask' from the average dynamic spectrum obtained by folding over many (> 500) periods. 'Pulse mask' is a 2-dimensional Boolean array with 'true' value where the pulse occurs and 'false' value elsewhere. Two methods were used in obtaining the 'pulse mask'. The first method takes the average dynamic spectrum as the only input and detects the pulse by using robust root mean square (RMS) error. Robust RMS error is obtained in a similar manner as robust mean; it excludes the 'outliers' in its calculations. After methods for appropriate refining and widening to accommodate for pulse signals which might have arrived slightly earlier/later than the average pulse, we obtain the 'pulse mask'. FIG 5.6 (a) shows an average dynamic spectrum while FIG 5.6 (b) shows it's corresponding 'pulse mask' obtained using this method.

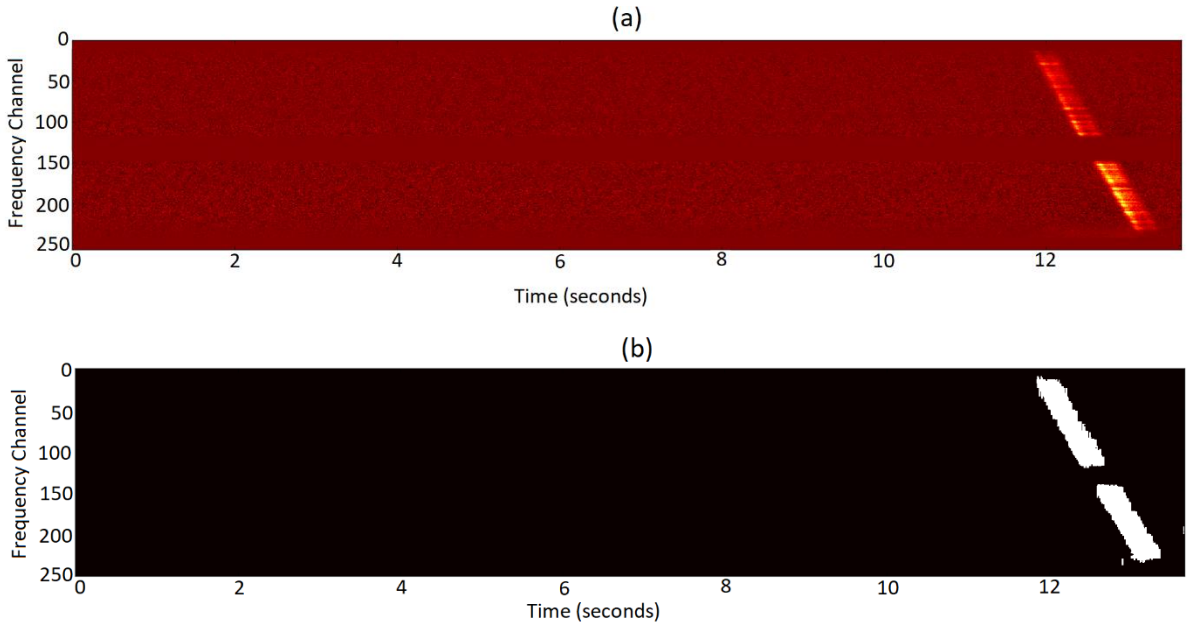

Fig 5.6: (a) a sample average Dynamic Spectrum (b) its Pulse Mask

The second method uses the fact that we know the Dispersion Measure and hence the dispersion delay at each frequency channel. It takes the Dispersion Measure, a reference channel, central position of the pulse in that channel and the pulse width as inputs to model a dispersed pulse which is then used as a mask. Such a 'pulse mask' and its corresponding average dynamic spectrum is shown in Fig 5.7(b) and 5.7(a) respectively.

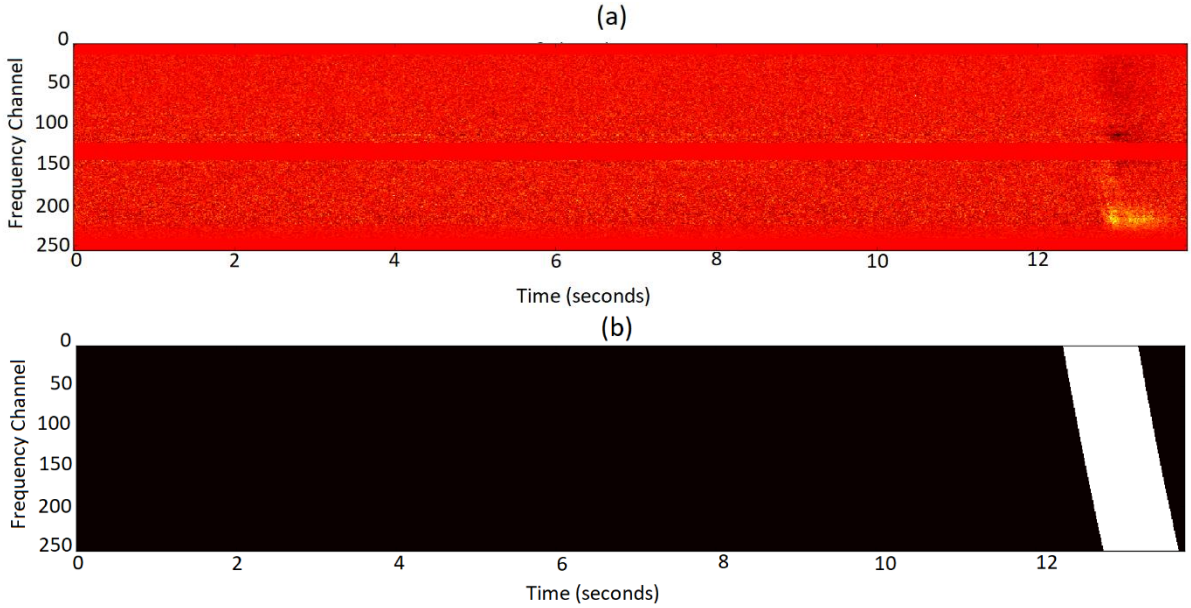

Fig 5.7: (a) a sample average Dynamic Spectrum (b) its modelled Pulse Mask

This pulse mask is then overlaid appropriately on the dynamic spectrum using the time at each column and the pulse period. Thus, we now know exactly where the pulse occurs in the dynamic spectrum.

We then calculate $T(f)$, $A(t_j)$ and $B(t_j)$ as follows:

- Template Spectrum ($T(f)$):
  -A more accurate template spectrum is obtained from the averaged dynamic spectrum by averaging all the spectra not containing the pulsar signal.
- Sum of non-pulse intensities in the Dynamic Spectrum ($A(t_j)$):
  -For each time column t_j, we sum over the intensities from all the non-pulse channels obtained from the pulse mask.
- Sum of non-pulse intensities in the Template Spectrum ($B(t_j)$):
  -We sum over the intensities of Template Spectrum $T(f)$ for the same non-pulse channels used to calculate $A(t_j)$.

The correction factor and the de-compressed dynamic spectrum are then obtained similarly to that in method 2.

$$c(t_j) = \frac{A(t_j)}{B(t_j)}$$

and

$$I_{de-compressed}(f_i, t_j) = \frac{I(f_i, t_j)}{c(t_j)}$$

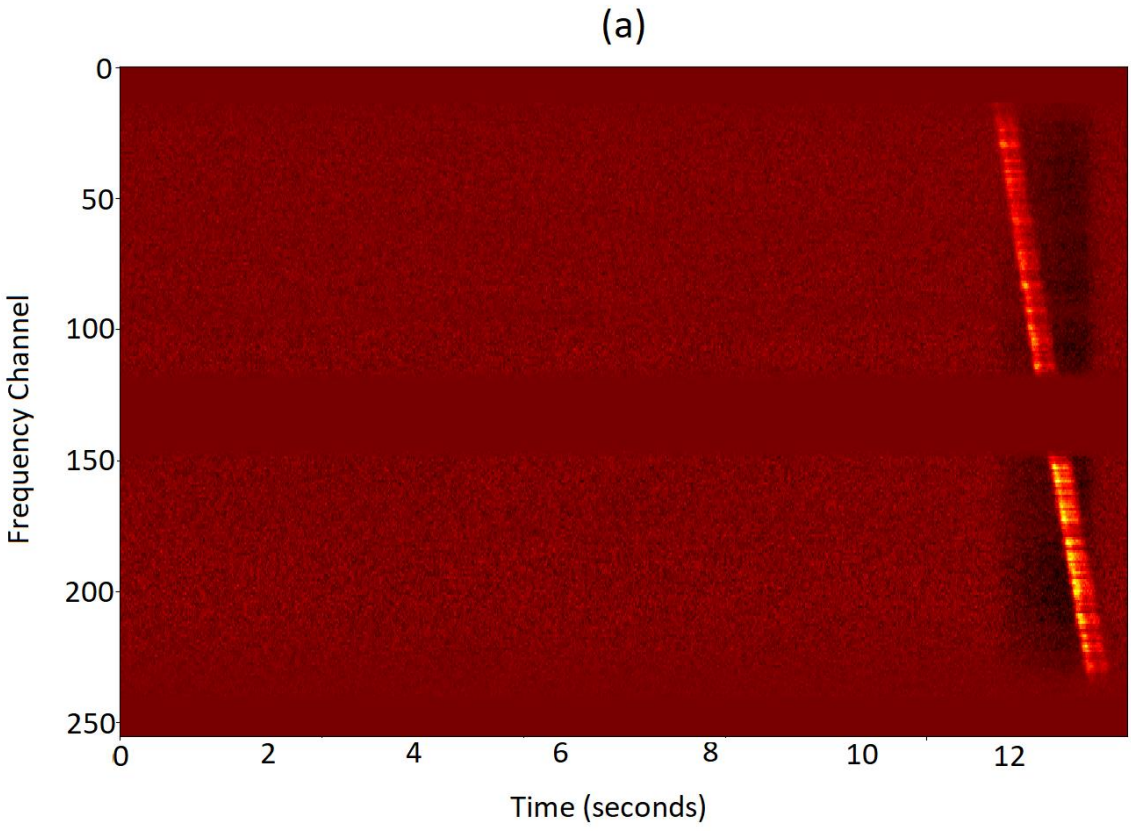

Fig 5.8: (a) Folded average Dynamic Spectrum in band 3 for B0834+06

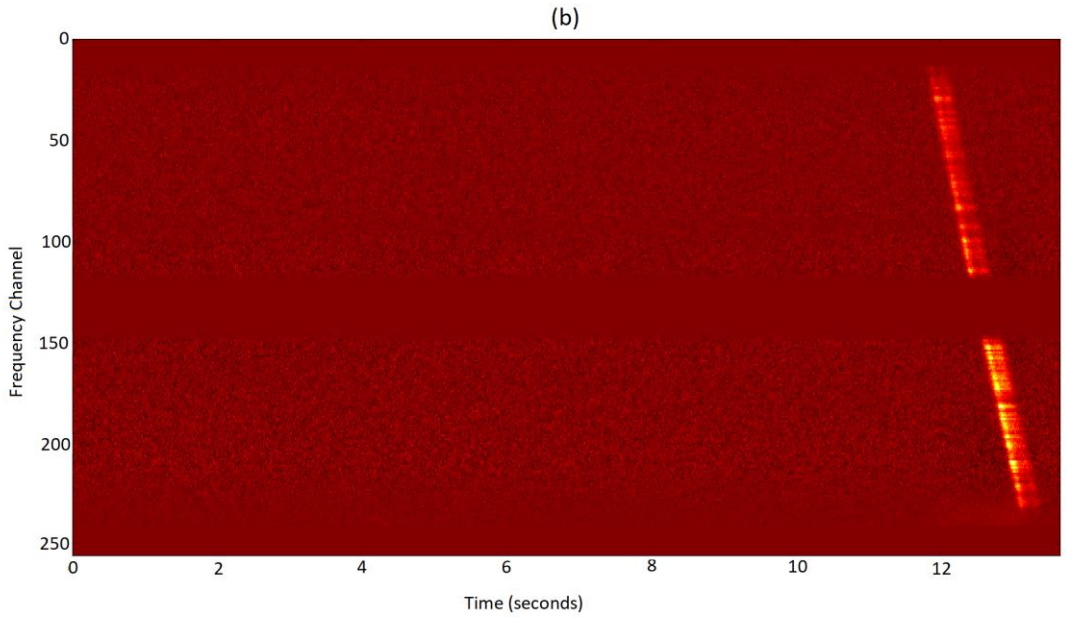

Fig 5.8: (b) De-compressed Dynamic Spectrum for this.
Note that the black band corresponding to the drop in intensities due to compression seen in figure (a) is completely fixed by de-compression using method 3 in figure (b).

This method is very robust and should work for pulsars with large DM (e.g., B0834+06) where the dispersion delay is more than the pulse width. This can be seen in Fig 5.8 (a) and (b), which shows the folded dynamic spectrum for this pulsar before and after de-compression using this technique. However, for pulsars with low DM, especially in higher frequencies where the dispersion delay is less than the pulse width, there are times in the on-pulse region where the entire spectrum consists the pulsar signal. In this case no comparison can be made and this method fails. This can be seen in Fig 5.9 which shows a band 3 (central frequency 233 MHz) dynamic spectrum for pulsar B0809+74 de-compressed using method 3.

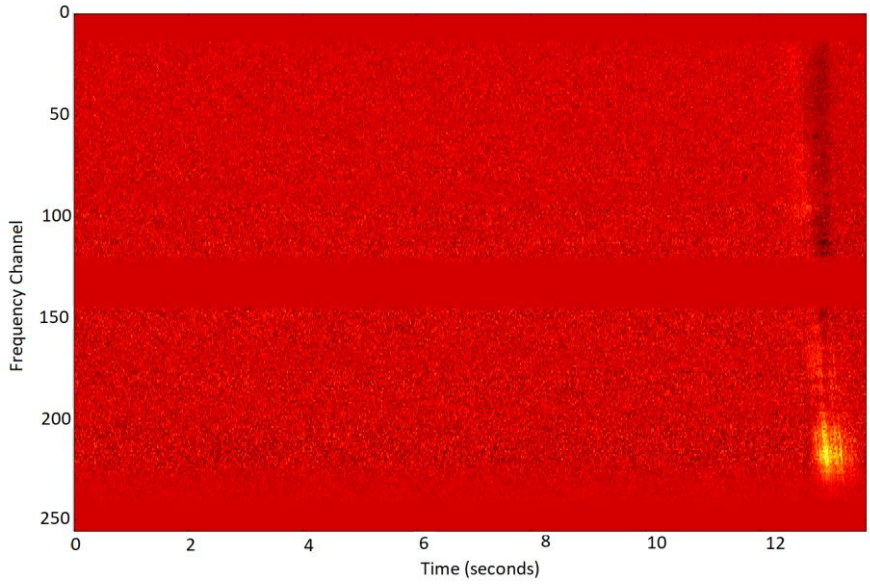

Fig 5.9: Failure of de-compression using method 3 seen in a low DM pulsar B0809+74.The dark band in on-pulse region corresponds to drop in intensities due to compression.

However, it was observed that this decompressed region is complementary to that used in method 2. Hence using both; method 2 and method 3, we get a completely de-compressed dynamic spectrum (Refer Fig 5.10).

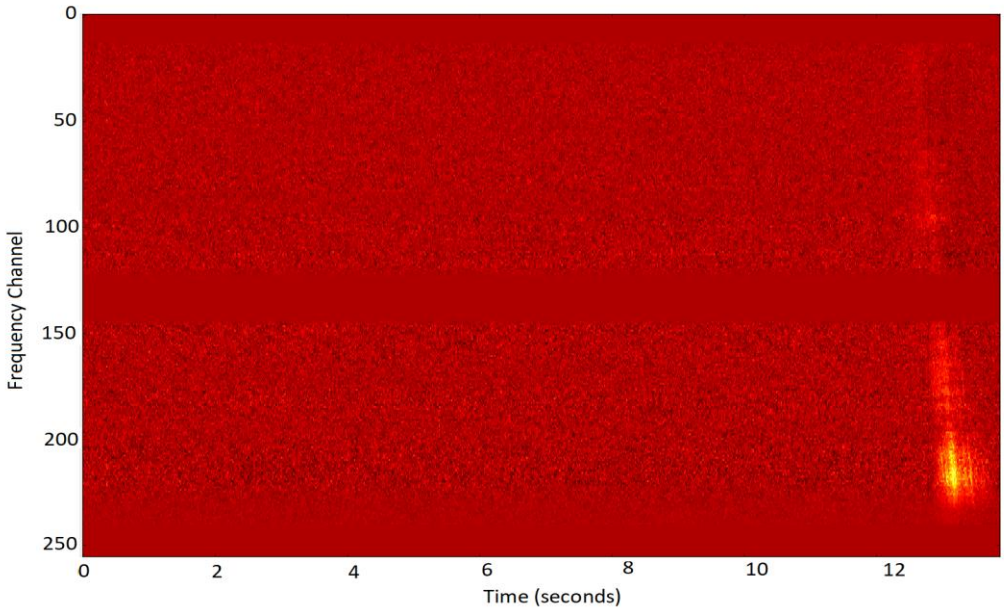

Fig 5.10: Completely de-compressed average dynamic spectrum for band 3 data of pulsar B0809+74 using both method 2 and method 3 of de-compression

Method 3 suffers from another drawback. Though it predicts the pulse position in the dynamic spectrum, it doesn't correct for compression caused by strong RFIs which can occur anytime and are hence unpredictable.

5.6 Method 4 – Using an unmodulated RFI signal:

This method would work only when there is a constant and unmodulated RFI which is present in at least one channel throughout the observation. Take the average intensity of this RFI signal over long time interval in a particular channel. This would serve as a reference intensity I_{ref}. We then use the fact that presence of any strong signal (including the pulsar signal) would also decrease the intensity of this RFI signal at that particular time. Let the RFI signal at time t_j be represented as $I(t_j)$. The correction factor and the corrected de-compressed dynamic spectrum can now be found as:

$$c(t_j) = \frac{I(t_j)}{I_{ref}}$$

And

$$I_{de-compressed}(f_i, t_j) = \frac{I(f_i, t_j)}{c(t_j)}$$

However, finding such a constant and unmodulated RFI signal present throughout the observation is rare. We haven't found such an RFI channel in our data and hence this method has not been implemented yet.

6. Investigating Sub-pulse Drift Parameters

Now that we have the single pulse stack with the sub pulse drifting phenomena clearly visible, we can proceed to investigate this phenomenon in detail. Initially, we notice that we can completely describe the sub pulse drifting by a set of three parameter; P_1, P_2 and P_3. Further analysis suggests that there is also a fourth parameter P_4. We shall talk about P_4 in detail later. For now, I shall describe the first three parameters.

P_1 (or just P) is simply what we call the period of the pulsar. It is rotation period of the pulsar and manifests as the time interval between two successive pulses. P_2 is the longitude separation between two drift bands at a particular period number. P_3 is the separation between the two bands in time taken at a certain longitude. It is generally represented in terms of P. Fig 6.1 shows all three parameters marked on a single pulse stack.

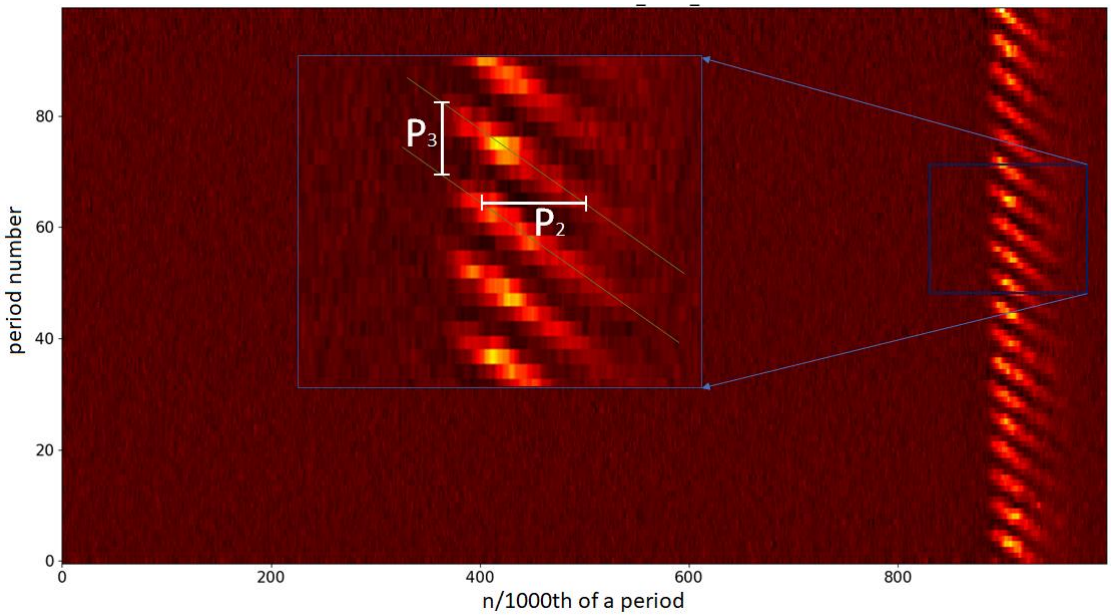

Fig 6.1: A sample sub-pulse drift sequence showing P_2 and P_3.

P_3 can be obtained as a fluctuation feature in the Longitude Resolved Fluctuation (LRF) spectrum as well as Harmonic Resolved Fluctuation spectrum. I shall now describe how we obtained LRF and HRF for pulsar B0809+74 and how we deduced P_3 (and also P_4).

Longitude Resolved Fluctuation Spectrum

First, we note the start and end longitudes for pulsar signals in the single pulse stack. In our case, the drift bands lie between 304.2 deg and 352.8 deg. For each longitude in this range,

we compute a 512-point Fourier Transform. This returns 512 complex values for each longitude. These 512 values are symmetric and only the first (or last) 256 values are chosen and squared to obtain a fluctuation power spectrum. Four such power spectra are averaged. This is done for each longitude in the selected range to get the fluctuation resolved power spectrum shown in the body of Fig 6.2**.**

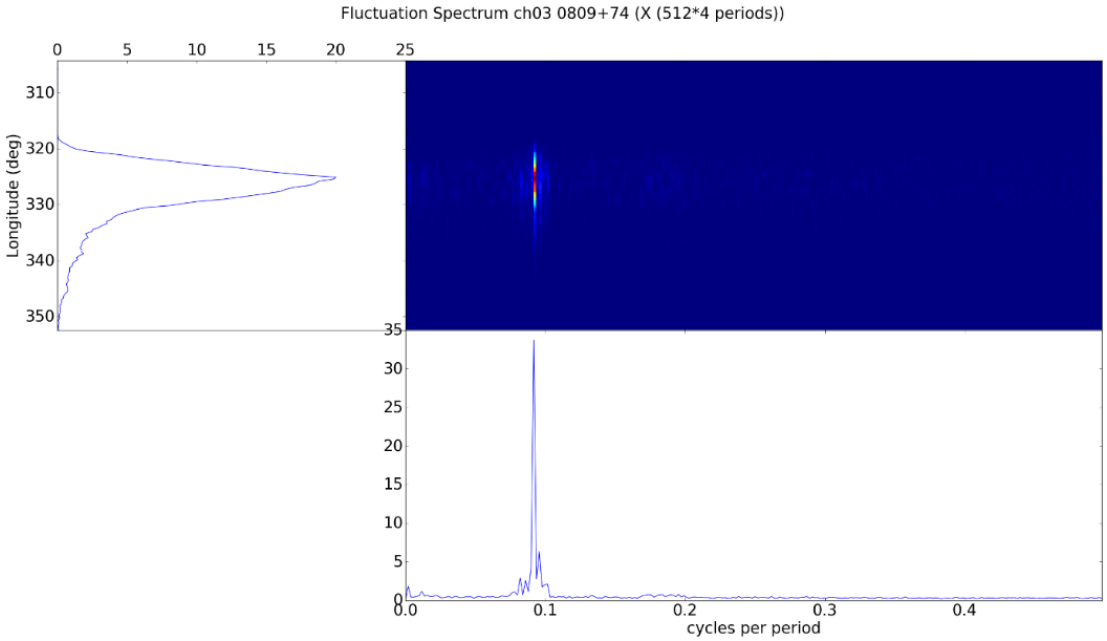

Fig 6.2: Longitude Resolved Fluctuation Spectrum for band 3 data of pulsar B0809+74

The first column of this LRF spectrum which corresponds to zero frequency is plotted on the left. It represents the average pulse profile. From this, we note that the average pulse has a width of about 30 deg in longitude. The longitude integrated LRF spectrum is plotted at the bottom. The fluctuation frequency on the horizontal axis is given in terms of cycles per pulsar period or simply (cP_1^{-1}). Here, we can see a primary fluctuation feature at $f_3 = 0.0917\ cP_1^{-1}$. Corresponding to this, we get $P_3 = 1/f_3 = 10.9$ periods per cycle. We can also see sidebands associated with the primary feature which we shall discuss later.

Harmonic Resolved Fluctuation Spectrum

In LRF spectrum, the fluctuations are sampled at just once a period. Hence it is possible that the observed feature might actually be an alias of fluctuations at frequencies larger than 0.5 cP_1^{-1}. To resolve this issue, we need to sample the fluctuations faster than once a period. To achieve this, we can exploit the fact that the signal is also sampled within the pulse width. For this purpose, we calculate the Harmonic Resolved Fluctuation (HRF) spectrum by unfolding the single pulse stack.

We modify our time sequence data such that the off-pulse signal is set to zero. This was achieved by simply retaining the values for on pulse longitudes (304.2 deg to 352.8 deg) while setting the values at other longitudes to zero before unfolding the single pulse stack. By unfolding, I mean obtaining a time sequence from the pulse stack by just placing successive periods one after another. This does not modify the spectral signatures of the pulsar signal.

Moreover, it reduces the noise, thereby increasing the Signal to Noise Ratio (SNR). We then take a Fourier transform for such a time sequence to obtain an unfolded fluctuation spectrum shown in Fig 6.3.

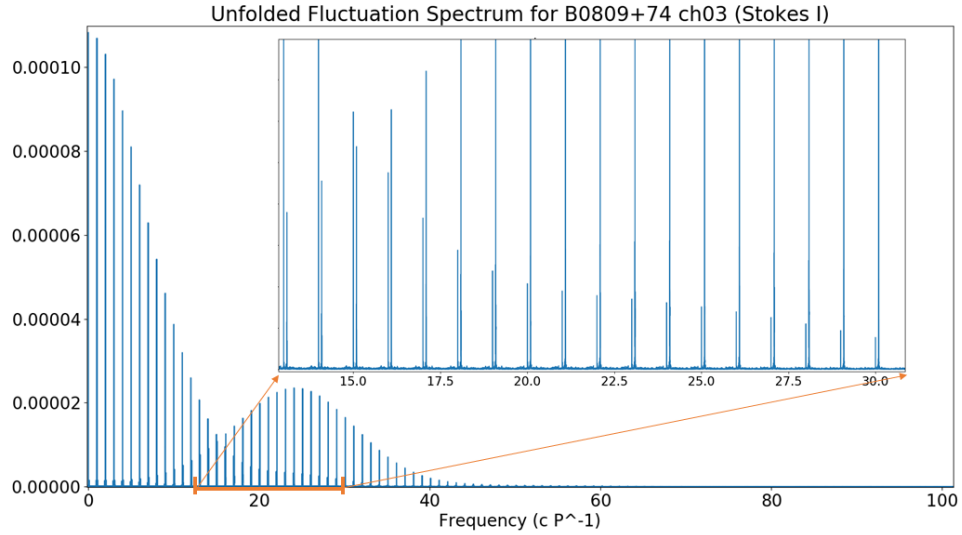

Fig 6.3: Unfolded Fluctuation Spectrum for band 3 of B0809+74

In this unfolded fluctuation spectrum, we can see features due to two sets of components. First, we see strong peaks corresponding to the harmonics at integral multiple of the pulsar rotation frequency (N cP_1^{-1} for N = 1,2,3 and so on). They are strongest at lower harmonics and decline rapidly for higher harmonics where they drop to (1/e) at about harmonic number 11. Here, we note that 360/11 ≈ 32 deg is approximately the width of the average pulse (seen in the left sub-plot of LRF Fig 6.2. The second set of components is seen between these fundamental peaks at slight off-sets; we can see features at (N + [0.091 ± 0.002] cP_1^{-1} for N=1,2,3 and so on) which increase gradually and reach a maximum for about harmonic number 24. We note that 360/24 = 15 deg, which is approximately P_2.

We obtain the HRF by simply stacking successive slices of 1 cP_1^{-1} from the unfolded fluctuation spectrum and stacking them one above another. This forms the body of HRF shown in Fig 6.4. The amplitude of the harmonics at integral multiple of pulsar rotation frequency is plotted on the left. The harmonic integrated HRF is plotted at the bottom. We see that the primary feature is at 0.091 ± 0.002 cP_1^{-1}. Hence the primary feature in LRF is indeed a non-aliased true feature. Now we can say that P_3 = 1/0.091 = 10.9 + 0.2 periods per cycle for certain. This implies that the drift band repeats itself after nearly 11 periods.

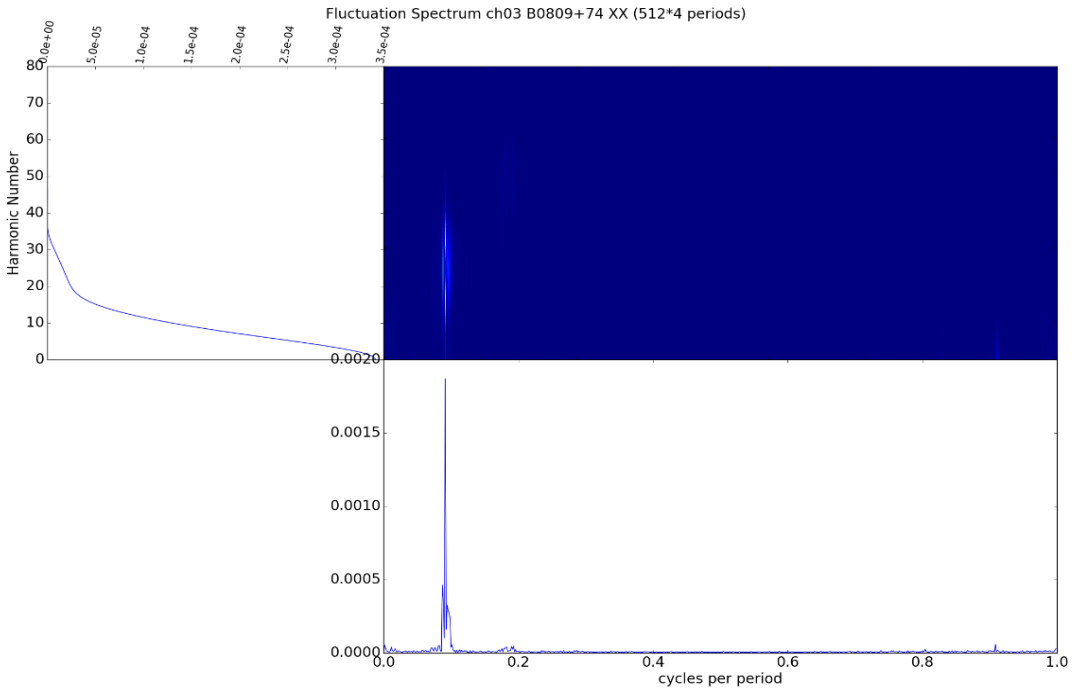

Fig 6.4: Harmonic Resolved Fluctuation Spectrum for band 3 data of pulsar B0809+74

Now that we have determined the three parameters defining sub pulse drift; P_1, P_2 and P_3, let us look back to the Ruderman-Sutherland picture of sub beams. Each of the sub pulse can be mapped to a sub-beam in the pulsar magnetosphere. The drift in the sub-pulse can then be explained by the rotation of sub beams around the magnetic axis of the pulsar. Naturally two questions arise; the number of such sub beams and the time taken by a sub beam for one rotation around the magnetic axis, also known as the circulation time. Both questions are not independent. If we use P_4 to denote the circulation time and fold the single pulse stack on P_4, we get a block averaged drifting sub pulse sequence shown in Fig 6.6. The number of drifting sub pulses in this is the same as the number of sub beams rotating around the pulsar magnetosphere. Inversely, we can also estimate P_4 by knowing the number of sub-beams.

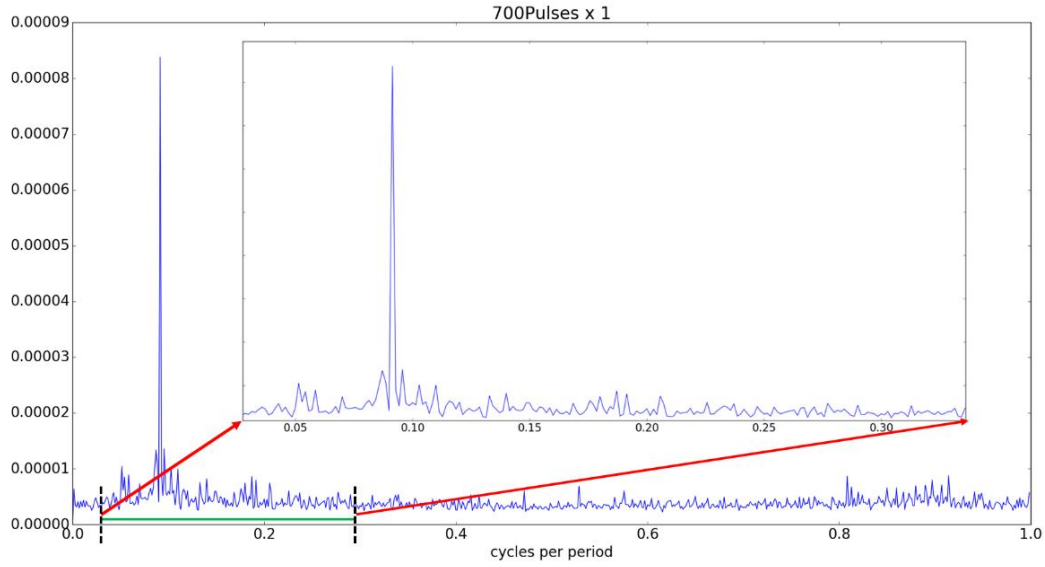

Fig 6.5: Harmonic Integrated HRF spectrum. Note the sidebands around the primary peak.

The number of sub-beams can be estimated by knowing the angular separation between two beams along the magnetic axis(η). η can be found out by simply by knowing the angular separation between the beams along the rotation axis, which is P_2. We can use the relation:

$$\sin\left(\frac{\eta}{2}\right) = \frac{\sin\left(\frac{P_2}{2}\right) \times \sin(\alpha + \beta)}{\sin|\beta|}$$

Where, α is the angle between the rotation and the magnetic axis and β is the angle between line of sight and the magnetic axis also called the impact angle. The geometry is shown in Fig 6.6.

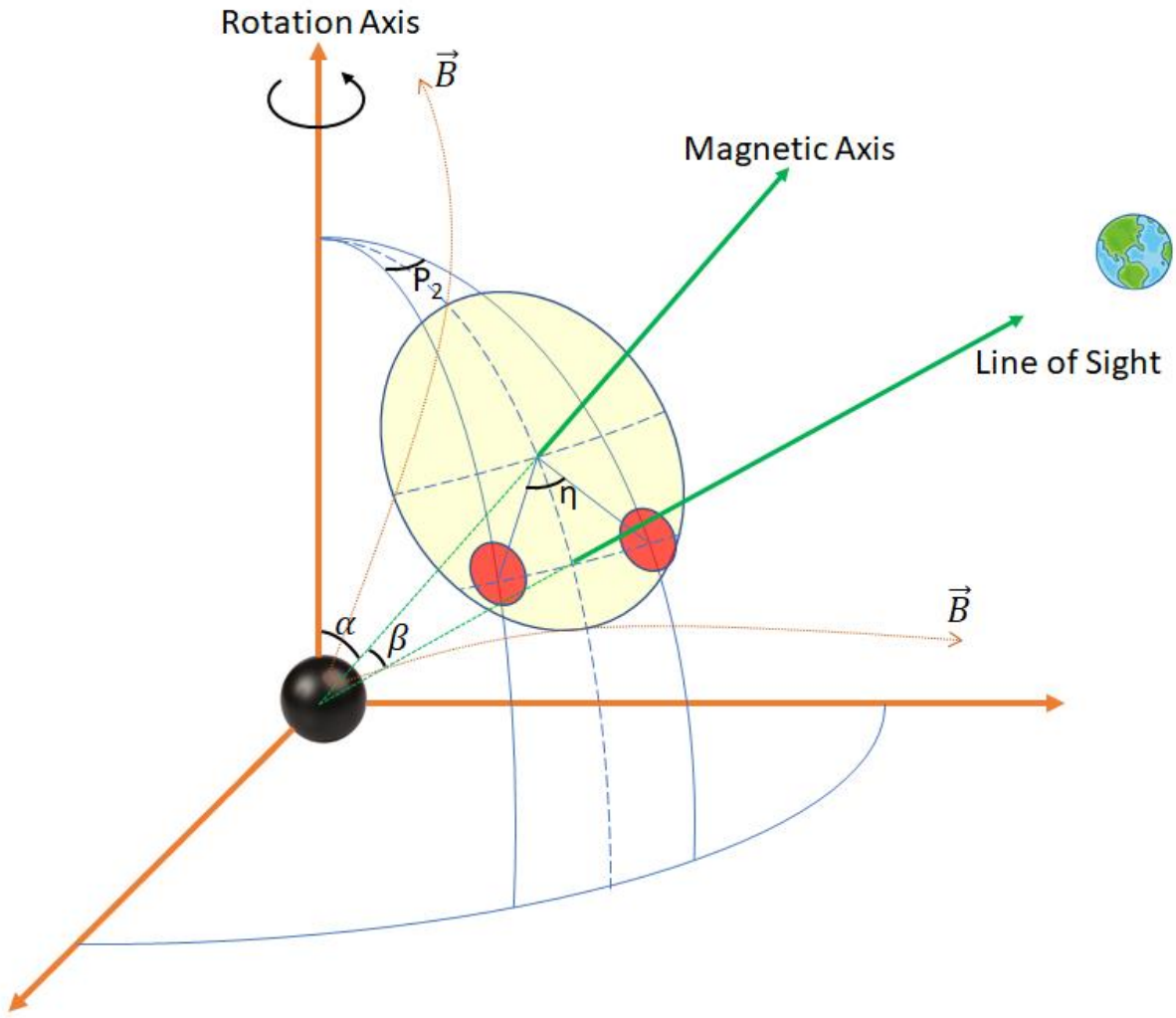

Fig 6.6: Schematic diagram showing pulsar geometry.
The pulsar is at the origin. The yellow shaded region is a cross section of the magnetosphere. Red regions represent sub-beams in the magnetosphere.

Once we know η, assuming the sub beams are equally spaced, (360/η) gives an estimate for the number of sub beams. P_3 times the number of sub-beams gives an estimate for P_4. Using this value of P_4, we search for nearby values. This was done by folding the single pulse stack for nearby P_4 and looking for P_4 with the maximum sum of squares of intensities in the obtained folded profile. The maximum sum of squares ensures we get the P_4 with the sharpest contrast in folded profile without any smearing.

For pulsar B0809+74, P_2 was found to be 12.6 deg. α and β for this pulsar are 9 deg and 4.5 deg respectively (Rankin J.M. et. al., "Phenomenology of pulsar B0809+74's rotating sub-beam system", 2006). This gives $\eta = 38.11$. This implies $360/\eta \approx 9.4$. Taking $(9 \times P_3) \approx 98.1$ as an approximate value for P_4, we plot the sum of squares for profiles folded using nearby P_4 values. Resulting plot is shown in Fig 6.7 below.

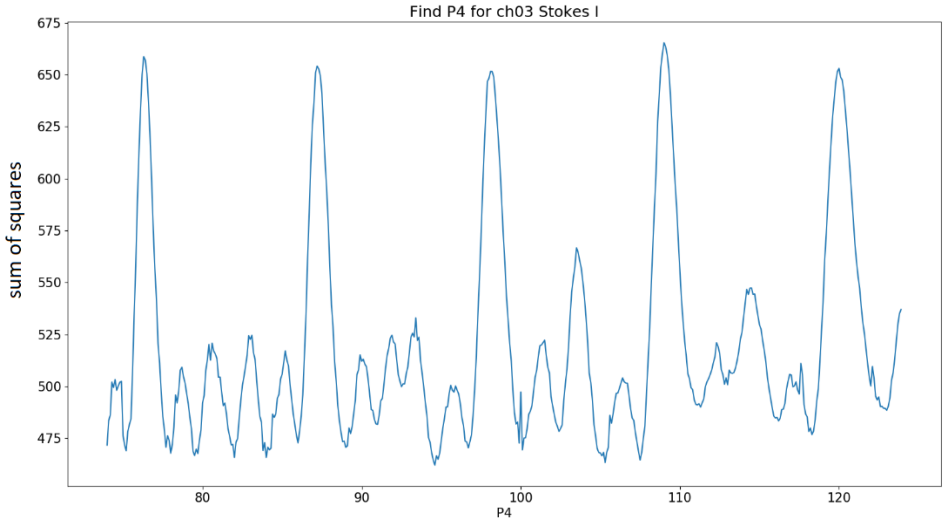

Fig 6.7: Sum of squares for P_4 folded profile vs P_4.
Notice that the peaks occur at integral multiples of P_3 and the maximum is at 109.03.
This means that N = 10 and not 9 as estimated earlier.

Once we know P_4, we can now find the P_4 folded profile in which each sub-pulse is associated with a beam rotating about the magnetic axis. A P_4 folded profile for Stokes I parameters for pulsar B0809+74 in band 03 (232 MHz) is shown in Fig 6.8**.** Note that this has 10 sub-pulses which correspond to 10 beams in the magnetosphere

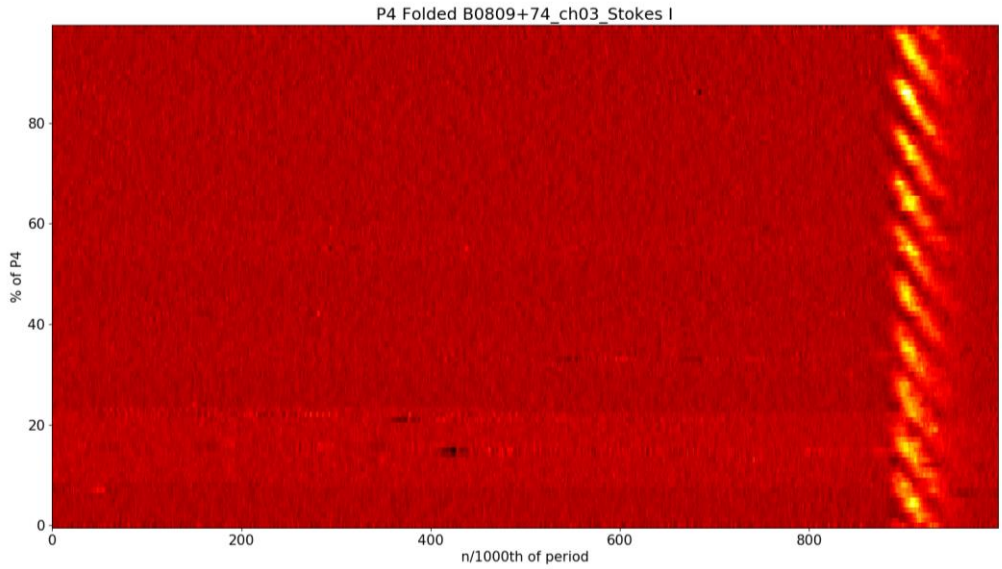

Fig 6.8: P_4 folded profile for stokes I parameter for band 3 of B0809+74.
Note that there are 10 sub-pulses which can be mapped to 10 sub-beams in the magnetosphere.

7. Shift in sub-pulses across bands

Now that we have obtained P_4 folded profiles in each frequency band, we can calculate the shift between the sub-pulse drift profile seen in each band. The well accepted relation between frequency of emission and the height of this emission zone in the magnetosphere can then be used to determine the latter. Hence, we now know shift as a function of height. This shift would tell us if there is any twisting of the dipolar magnetic field.

For this, we simply calculate the cross correlation between the P_4 folded profiles. The result of cross correlation between P_4 folded profiles for band 2 (172 MHz) and band 3 (233 MHz) is shown in Fig 7.1.

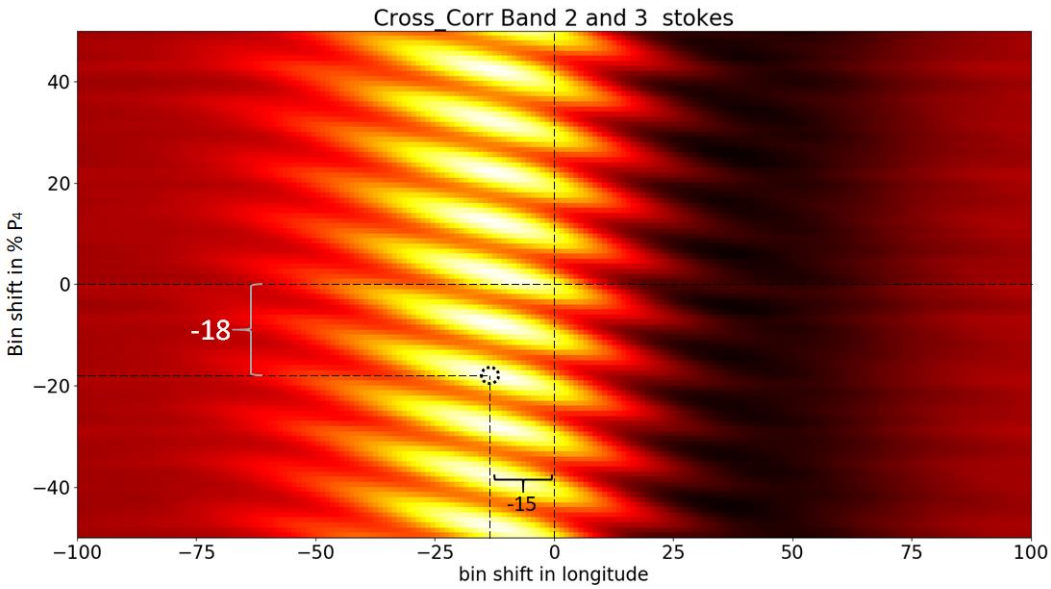

Fig 7.1: Cross correlation of P_4 folded profiles of band 2 and band 3.
Note that the bin shift of -18 along fraction of P_4 implies a shift of
(-18*360/100) = 64.8 deg between the sub-beams in the magnetosphere.

As can be seen, the peak of the cross correlation is not centred at the origin. It is shifted by 18 bins along the % of P_4 axis. 18 bins correspond to (18*360/100) = 64.8 deg. This implies that there is a twist in pulsar magnetosphere which is seen as a shift of 64.8 deg in the sub beams in cross section of magnetosphere at heights corresponding to 172 MHz and 233 MHz.

A similar analysis needs to be carried out in other bands with. For pulsar B0809+74, Band 1 is polluted with lot of RFI. Band 4 has a weak signature of the pulse. No pulse is observed for higher frequency bands. Further, we can repeat the whole analysis for other drifter pulsars as well.

8. Change in P_3 observed over the observation time

Just by looking at the single pulse stack for ≈ 2400 periods of data in band 3 for B0809+74, we see that the pulsar behaviour changes after about 700 periods. From 0 to 700 periods, the drift bands are strong and well defined. Here, P_3 was found to be 1/0.0917 = 10.90 periods per cycle and the P_3 folded profile showed a strong and well-defined drift band as shown in Fig 8.1. However, analysis using same P_3 for subsequent pulses (pulse number 700 to 1500) didn't produce a sharp profile (seen in Fig 8.2). Hence, we investigate for any changes in P_3.

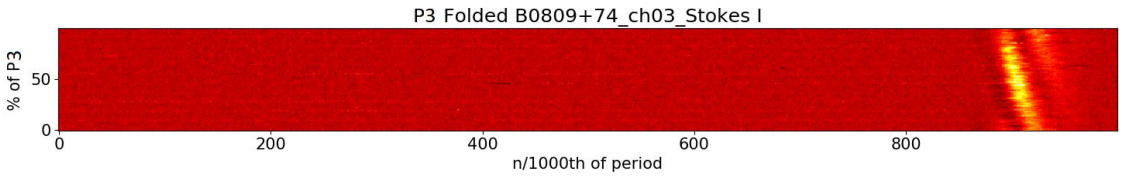

Fig 8.1: P_3 folded profile for first 700 pulses in band 3 (233 MHz) using P_3=1/0.0917 cP_1^{-1} for B0809+74. Note the well-defined profile without any smearing.

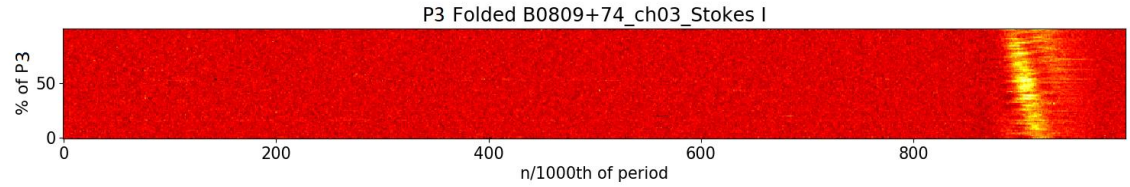

Fig 8.2: P_3 folded profile for pulse numbers 700 to 1500 in band 3 (233 MHz) using P_3=1/0.0917 cP_1^{-1} for B0809+74. Note the smearing which indicates incorrect value of P_3.

First, we plot integrated HRF for band 3 of B0809+74 for pulse numbers 0 to 700 (Fig 8.3a), and 1500 to 2100 (Fig 8.3b).

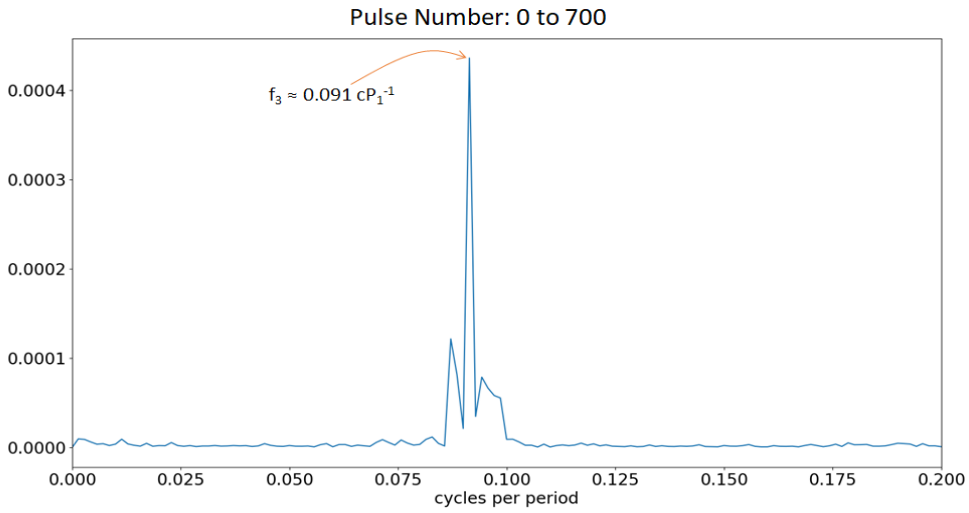

Fig 8.3 (a): Integrated HRF for initial part of the observation from pulse numbers 700 to 1500 in band 3 (233 MHz) for B0809+74.
The feature is seen at f_3 = 0.0917 cP_1^{-1}.

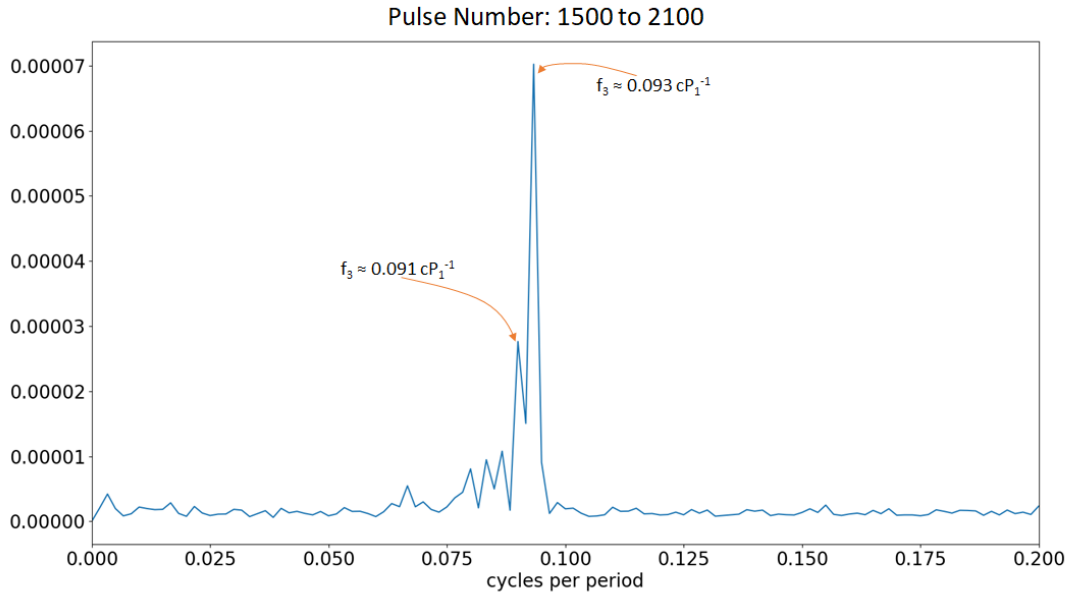

Fig 8.3 (b): Integrated HRF for later part of the observation from pulse numbers 1500 to 2100 in band 3 (233 MHz) for B0809+74. The feature is seen at $f_3 \approx 0.093\ cP_1^{-1}$.

For pulse number 0 to 700, we see a single feature which peaks at $f_3 = 0.091 \pm 0.002\ cP_1^{-1}$ as expected. It is more interesting to see the integrated HRF for pulse number 1500 to 2100 where the only one peak is seen, that too not at $f_3 = 0.091 \pm 0.002\ cP_1^{-1}$ but at $f_3 = 0.093 \pm 0.002\ cP_1^{-1}$. Similar behaviour is seen in band 2 as well as band 3. On searching for f_3 values in the vicinity of $0.093\ cP_1^{-1}$ by maximizing the sum of squares of folded profile using this f_3, we got a more accurate value of $P_3 = 1/0.0935 = 10.69$ periods per cycle. This change in P_3 can be confirmed by folding the data for later pulse numbers (1500 to 2100) on both values of P_3; $1/0.0917\ cP_1^{-1} = 10.90$ periods per cycle and $1/0.0935\ cP_1^{-1} = 10.69$ periods per cycle. The results of this folding are shown in Fig 8.4.

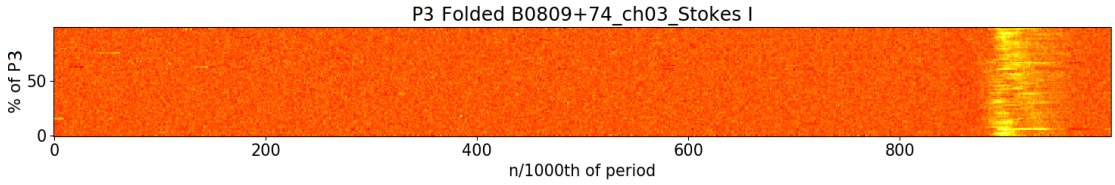

Fig 8.4 (a): P_3 folded profile for pulse number 1500 to 2100 in band 3 (233 MHz) using $P_3 = 10.90$ periods per cycle for B0809+74.
Note the smearing which indicates incorrect value of P_3.

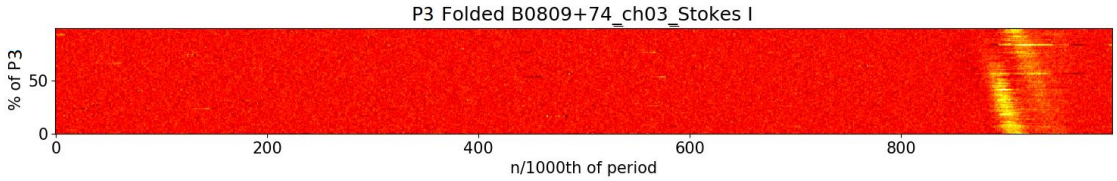

Fig 8.4 (b): P_3 folded profile for pulse number 1500 to 2100 in band 3 (233 MHz) using P_3 = 10.67 periods per cycle for B0809+74.
Note the well-defined profile without any smearing.

From this figure, the smeared P_3 folded profile for P_3 = 10.90 periods per cycle indicates that this P_3 is not acceptable. However, the sharp and well-defined P_3 folded profile for P_3 = 10.67 periods per cycle indicates that P_3 has indeed changed to this value for later part of the observation.

A more detailed study for the variation of P_3 for smaller steps of pulse numbers (say 100 periods instead of 700 used in the analysis done above) needs to be done.

Conclusion

After proper pulsar data analysis which includes packet synchronization, dispersion delay synchronization between bands, dynamic spectra for both polarizations, RFI detection and subsequent rejection of the data, de-compression, de-dispersion, obtaining time series, a single pulse stack was obtained for pulsar B0809+74 in bands 2(172 MHz), 3(233 MHz) and 4(330 MHz) using the data obtained from the RRI-GBT Multi Band Receiver.

This single pulse stack was then used to obtain Longitude Resolved Fluctuation (LRF) spectrum and Harmonic Resolved Fluctuation (HRF) spectrum. LRF and HRF were then used to determine the sub-pulse drift parameters $P_3 \sim 11$ periods and $P_4 \sim 109$ periods. Subsequently, a P_3 and P_4 folded sub-pulse drift profile was obtained. The analysis was repeated for band 2 (172 MHz) and band 4 (330 MHz). No pulse signatures were observed for band 5 onwards. Band 1 suffers from a lot of RFI.

From the P_4 folded profile, we find 10 sub-pulses. This implies 10 sub-beams rotating around the magnetic axis of pulsar B0809+74.

Cross correlating the P_4 folded profiles in band 2 and band 3, we observe a shift of 64.8 deg. This implies there is a twist in the dipolar magnetic field of the pulsar that causes this shift in the sub-beams at heights. (Note that the height of emission in the magnetosphere can be obtained by the well accepted Radius to Frequency Mapping.)

References

- Backer D. C., “Pulsar Fluctuation Spectra and the Generalized Drifting sub-pulse Phenomenon”, 1973, ApJ, 182, 245
- Ruderman M. A., & Sutherland P. G., “Theory of Pulsars: Polar Gaps, Sparks, and Coherent Microwave Radiation”, 1975, ApJ, 196, 51
- Deshpande A. A., & Rankin, J. M., “Pulsar Magnetospheric Emission Mapping: Images and Implications of Polar Cap Weather”, 1999, ApJ, 524, 1008
- Maan, Y., & Deshpande A. A., “Inter-relationship between the two emission cones of B1237+25”, 2014, ApJ, 792, 130
- Maan, Y., et. al., “RRI-GBT Multi-Band Receiver: Motivation, Design and Development”, 2013, ApJ, 204, 12
- Deshpande A. A., & Rankin J. M., “The topology and polarization of sub-beams associated with the `drifting' sub-pulse emission of pulsar B0943+10 - I. Analysis of Arecibo 430- and 111-MHz observations”, 2001, MNRAS, 322, 438